Monthly Notices of the ROYAL ASTRONOMICAL SOCIETY

MNRAS **515,** 2305–2321 (2022)
Advance Access publication 2022 June 24

https://doi.org/10.1093/mnras/stac1746

Weak-lensing magnification of Type Ia supernovae from the Pantheon sample

Paul Shah [1]★ Pablo Lemos[1,2] and Ofer Lahav[1]

[1]*Department of Physics and Astronomy, University College London, Gower Street, London WC1E 6BT, UK*
[2]*Department of Physics and Astronomy, University of Sussex Brighton BN1 9QH, UK*

Accepted 2022 June 20. Received 2022 June 13; in original form 2022 March 18

ABSTRACT

Using data from the Pantheon Type Ia supernovae (SN Ia) compilation and the Sloan Digital Sky Survey, we propose an estimator for weak-lensing convergence incorporating positional and photometric data of foreground galaxies. The correlation between this and the Hubble diagram residuals of the supernovae has 3.6σ significance, and is consistent with weak-lensing magnification due to dark matter haloes centred on galaxies. We additionally constrain the properties of the galactic haloes, such as the mass-to-light ratio Γ and radial profile of the halo matter density $\rho(r)$. We derive a new relationship for the additional rms scatter in magnitudes caused by lensing, finding $\sigma_{\rm lens} = (0.06 \pm 0.017)(d_{\rm C}(z)/d_{\rm C}(z=1))^{3/2}$, where $d_{\rm C}(z)$ is the comoving distance to redshift z. Hence, the scatter in apparent magnitudes due lensing will be of the same size as the intrinsic scatter of SN Ia by $z \sim 1.2$. We propose a modification of the distance modulus estimator for SN Ia to incorporate lensing, which can be easily calculated from observational data. We anticipate this will improve the accuracy of cosmological parameter estimation for high-redshift SN Ia data.

Key words: gravitational lensing: weak – transients: supernovae – cosmology: dark matter – galaxies: haloes – cosmology: cosmological parameters.

1 INTRODUCTION

Type Ia supernovae (SN Ia) are used extensively in cosmology as standard candles, due to an empirical relation between their absolute magnitudes and observable light-curve properties (Phillips 1993; Tripp & Branch 1999). Their high luminosities allow them to be observed out to redshift $z \sim 2$ (Riess et al. 2018). Thus, they serve as a key cosmological resource, connecting the expansion history of the universe from when it was matter-dominated, through to the current epoch of dark energy domination.

The relative luminosities of SN Ia may be assembled in a Hubble diagram and used to constrain cosmological parameters such as the matter density $\Omega_{\rm M}$ and the equation of state of dark energy w in simple extensions of Λ cold dark matter (ΛCDM; Scolnic et al. 2018). If their absolute magnitude is calibrated, the Hubble constant H_0 may be determined (e.g. see Freedman et al. 2019; Lemos et al. 2019; Riess et al. 2021, and for a review of the distance ladder, see Shah, Lemos & Lahav 2021).

However, for supernovae to be accurate and unbiased distance estimators, the scatter of their observed magnitudes must be well characterized. Gravitational lensing forms an important part of the scatter because it is an effect that increases with distance. Treated as random scatter, it therefore degrades the precision of survey data (Holz & Linder 2005). Also, for magnitude-limited surveys, the calculation the Malmquist bias correction requires an understanding of the sources of scatter (Kessler & Scolnic 2017). Therefore, to make the most of modern high-redshift SN Ia data sets, it is essential to understand lensing magnification.

Gravitational lensing can also be used as a cosmological probe in its own right. The lensing signal is sensitive to the amount, distribution, and type of dark matter. For example, Metcalf & Silk (1999) and Seljak & Holz (1999) examined the case of dark matter being a mixture of weakly interacting massive particles or massive compact halo objects (MACHOs; e.g. black holes). They showed that the skew of the lensing probability distribution function (pdf), proxied by the difference between the mode and the mean, is sensitive to $\Omega_{\rm m}$ and Ω_Λ independently, but most sensitive to the form of dark matter. They argued that even a modest sample of 100 SN Ia would be sufficient to constrain the fraction of MACHOs to within 20 per cent. In a similar argument, Hada & Futamase (2016) show how SN Ia magnification may be used to bound the sum of neutrino masses. Going further, the moments of the lensing pdf may be fitted by simulations to the power spectrum of matter density fluctuations (Marra, Quartin & Amendola 2013). This is particularly interesting in the context of moderate tensions that have arisen between measurements of the power spectrum normalization σ_8 from the cosmic microwave background (CMB) and galaxy surveys (see e.g. Lemos et al. 2021; Tröster et al. 2021).

Gravitational lensing magnification is also complementary to time-delay and shear lensing studies, which have been used to measure the Hubble constant H_0 (Wong et al. 2020), and build maps of foreground mass (Oguri et al. 2018; Giblin et al. 2021; Jeffrey et al. 2021). However, these studies have some drawbacks. They are distance-limited, as the shape of the galaxy must be resolved for it to work. Nuisance parameters and some bias may be introduced by an intrinsic alignment model. They are low resolution, and require

★ E-mail: paul.shah.19@ucl.ac.uk

sufficient numbers to average over. Lastly, they suffer from the 'mass-sheet degeneracy' whereby the cosmological parameters, but not the lensing observables, are changed by the addition of a matter sheet of constant density along the line of sight (LOS; see section 5.2 of Bartelmann & Schneider 2001). A measurement of the absolute magnification of a background source breaks this degeneracy (Falco, Gorenstein & Shapiro 1985).

SN Ia seem ideal for magnification studies as, once standardized, their luminosities have an intrinsic scatter of $\sigma_{\rm int} \simeq 0.1$ mag. Also, SN Ia can be seen at distances great enough for the magnification to be measurable. The scatter caused by magnification is thought to be $\sigma_{\rm lens} = 0.04z$–$0.09z$ mag, where z is the redshift, on the basis of simulations (Frieman 1997; Holz & Linder 2005; Marra et al. 2013). A small number of well-magnified SN Ia with $\Delta m < -0.25$ mag are expected. However, four problems exist in observing it. First, existing survey numbers peak at $z \sim 0.3$ where the magnification is likely to be small. Secondly, SN Ia are rare, transient events, so the sample to work with is smaller by two orders of magnitude compared to galaxy or quasar samples. Thirdly, the analysis must be centred around the set of sources, rather than lenses (as weak-lensing surveys are), so it is 'pot luck' what lies close to the LOS. Additionally, the limiting magnitude (also known as the *detection efficiency*) of a supernova survey is not so straightforward to determine, meaning biases are harder to estimate. Lastly, it is far from certain that a limited set of SN Ia would fairly sample the distribution of magnification, and selection processes could obscure its effect (we expand on this further in Section 5).

Observational studies of SN Ia magnification have been made by some authors. Jönsson et al. (2010) used 175 SN Ia from the Supernova Legacy Survey (SNLS) to detect magnification at a confidence of $\sim 1.4\sigma$, and estimated that lensing contributes an extra dispersion of $\sigma_{\rm lens} = 0.055z$ mag to supernovae. This value continues to be used in most cosmological analyses involving SN Ia, notably by the SH0ES team (Riess et al. 2021) in estimating H_0, and is embedded in Pantheon SN Ia data (Scolnic et al. 2018). Smith et al. (2014) combined a larger sample of 608 Sloan Digital Sky Survey (SDSS) SN Ia with number counts of a homogeneous sample of foreground galaxies. The authors also found a detection significance of $\sim 1.4\sigma$. Macaulay et al. (2020) used SN Ia and galaxies from the Dark Energy Survey (DES) 1Y data to compute the skew of the magnitude distribution (assuming intrinsic scatter is Gaussian, the skew may be attributed to lensing) with a simulated fit given by Marra et al. (2013) to derive a constraint on the matter power spectrum, and report a $\sim 1.3\sigma$ detection of magnification.

In this paper, we have two main goals. First, we seek to establish lensing is occurring with more certainty and measure its scatter. Secondly, we aim to constrain the mass and profile of galactic dark matter haloes within our chosen modelling framework. Adopting a Bayesian approach, we test a two-parameter family of physically motivated halo profiles, including the Navarro–Frenk–White (NFW; Navarro, Frenk & White 1996) and Hernquist (Hernquist 1990) profiles as special cases. We calculate posterior distributions of the parameters that describe our haloes.

Our paper is organized as follows. In Section 2, we derive the magnification in the weak-lensing regime of our halo profile, and connect this to lensing over cosmological distances. In Section 3, we describe our data and selection criteria. In Section 4, we specify our estimator for lensing convergence, what observables we will correlate, and our Bayesian model. Results are presented in Section 5, which we compare to the literature. We summarize our results in Section 6. A future paper will be devoted to cosmological parameters derived using SN Ia lensing. We retain factors of c in equations.

2 LENSING MODEL

2.1 Weak lensing by haloes

For extended matter distributions, it is useful to adopt the lensing potential formalism of Schneider (1985), for which we state the relevant formulae in this subsection. The *convergence* is defined as

$$\kappa = \frac{\Sigma\left(\boldsymbol{\theta}\right)}{\Sigma_{\rm c}}\,, \tag{1}$$

where the *surface density* is

$$\Sigma(\boldsymbol{\theta}) = \int \rho(\boldsymbol{\theta}, z){\rm d}z\,, \tag{2}$$

and the *critical surface density* is

$$\Sigma_{\rm c} = \frac{D_{\rm s}}{D_{\rm d}D_{\rm ds}}\frac{c^2}{4\pi G}. \tag{3}$$

Here, $D_{\rm d}$, $D_{\rm s}$, and $D_{\rm ds}$ are the angular diameter distances to the lens, source, and between lens and source, respectively.

We define $\delta m = m_{\rm lens} - m_0$ as the change in magnitude of a source due to a single lens, relative to the background cosmology in the absence of the lens. When the magnification is small, it may be taken to first order in the convergence and shear γ as

$$\delta m = -(5/\log 10)\kappa + O\left(\kappa^2, \gamma^2\right)\,. \tag{4}$$

Hence, we can compute the magnification expected from a galactic halo of a given density profile $\rho(r)$ by the following recipe:

(i) Obtain the critical density $\Sigma_{\rm c}$ from the angular diameter distances $D_{\rm ds}$, $D_{\rm s}$, and $D_{\rm d}$ in the background cosmology by equation (3).
(ii) Calculate the surface density Σ from equation (2) and convergence κ from equation (1).
(iii) Use equation (4) to calculate the magnification.

We note two important points. First, magnification is a concave function of the distance from the observer to the lens; hence, when magnification is strongest, it will be relatively insensitive to moderate errors in the distances (the gradient of magnification with lens distance will be small); this will be helpful when using distances derived from photometric redshifts. Secondly, as magnification is inversely proportional to (a power of) the impact parameter b via equation (2), its distribution will be skewed towards high magnification. Therefore, the commonly used assumption of Gaussian scatter in SN Ia residuals is not correct.

Equation (4) is valid to first order in the gravitational potential Φ/c^2, the light deflection angle α, and the convergence κ. These assumptions can be expected to hold for lensing by extended diffuse haloes; Jönsson et al. (2010) have checked the validity of this against ray tracing around such halo types, finding the difference to be less than 5 per cent. We have also checked that including shear for the NFW halo does not change our results.

2.2 Halo model

We define a double-power-law halo with profile

$$\rho\left(r; \gamma, \beta\right) = \frac{\delta_{\rm c}\rho_{\rm c}}{\left(\frac{r}{r_{\rm s}}\right)^{\gamma}\left(1 + \left(\frac{r}{r_{\rm s}}\right)\right)^{\beta}}\,, \tag{5}$$

where $\rho_{\rm c} = 3H(z)^2/8\pi G$ is the critical density of the universe at redshift z, $\delta_{\rm c}$ is a density parameter, and $r_{\rm s}$ is the *scale radius*. Our data will not have sufficient resolving power to constrain the inner

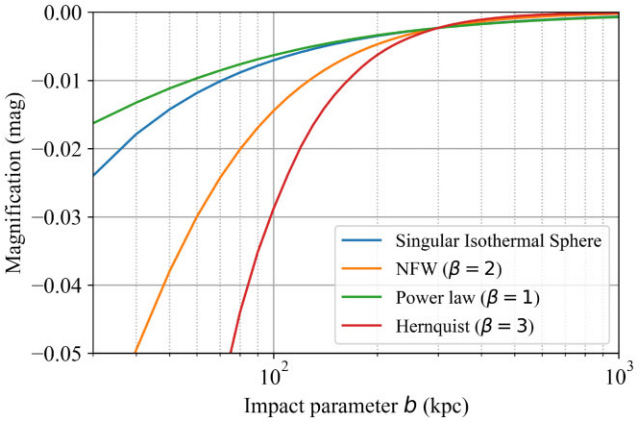

Figure 1. The magnification δm (in units of magnitude) by a typical galaxy of absolute magnitude $M = -21.25$ located at $z = 0.2$, of a source located at $z = 0.5$. The mass of each halo profile has been normalized to give the same observed magnification at $b = 300$ kpc, about the magnification-weighted average of our data sample. Although SN Ia LOSs passing within 100 kpc of a lensing galaxy centre are rare, we obtain the most constraining power from them.

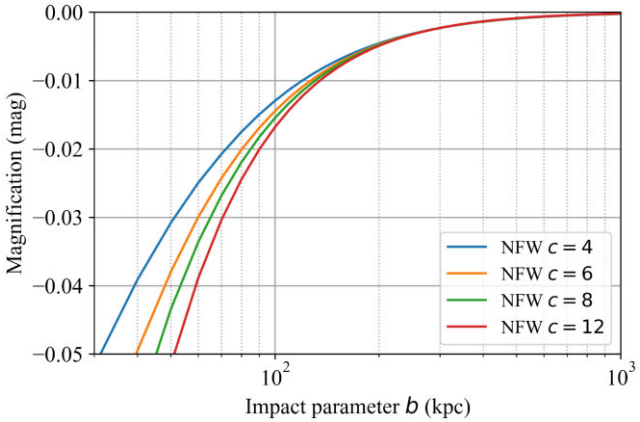

Figure 2. The magnification (in units of magnitude) due to a typical galaxy as detailed in Fig. 1. Here, we illustrate the NFW profile magnification at different values of the concentration parameter c, again normalizing to the same observed magnification at $b = 300$ kpc. It is evident from the graph that c will only be weakly constrained by our data .

slope γ, so we fix $\gamma = 1$ and leave β as a free parameter. Then, at small radii $\rho \propto r^{-1}$, whereas at large radii $\rho \propto r^{-1-\beta}$.

Standard spherical collapse theory implies that a sphere of radius r_{200} with average density $\bar{\rho} = 200\rho_c$ may be considered gravitationally bound. The scale radius r_s is then defined relative to r_{200} as

$$r_s = r_{200}/c, \tag{6}$$

where $c \simeq 5$–15 is the *concentration*,[1] which we take as a second free parameter. We make r_{200} a function of the mass $M_{200} = M(r < r_{200})$ it encloses

$$M_{200} = \frac{800\pi}{3}\rho_c r_{200}^3, \tag{7}$$

from which we obtain $\delta_c = \frac{200}{3}c^3 f(c)$, where

$$f(c) = \begin{cases} \frac{1}{c - \ln(c+1)} & \beta = 1 \\ \frac{1}{\ln(1+c) - c/(1+c)} & \beta = 2 \\ \frac{(\beta-2)(\beta-1)}{(1-(c+1)^{1-\beta}((\beta-1)c+1))} & \beta \neq 1, 2 \end{cases} . \tag{8}$$

Note that $\beta = 2$ corresponds to the NFW profile (Navarro et al. 1996), and $\beta = 3$ is the Hernquist profile (Hernquist 1990). The convergence and shear have analytical formulae for integer β, and we state those formulae (which have been derived in the literature) together with that for a singular isothermal sphere (SIS) in Appendix A.

For general β, we must obtain the surface density numerically. This is simplified by making the substitution $t = \sqrt{r/(r + r_s)(x + 1) - x}$, which results in

$$\Sigma(x; \beta) = 4\delta_c \rho_c r_s (x+1)^{\frac{1}{2}-\beta} \int_0^1 \frac{\left(1 - t^2\right)^{\beta-1}}{\sqrt{(1-x)t^2 + 2x}} \mathrm{d}t \ , \tag{9}$$

where

$$x = b/r_s \tag{10}$$

is the dimensionless impact parameter in units of the scale radius. We illustrate the magnification calculation for a range of our halo profiles in Figs 1 and 2.

[1]Any potential confusion with the speed of light c should be clear from the context.

We may expect many galaxies to lie at large distances from the LOS, so it is worthwhile to examine the lensing profile at large x. Taking the limit of equation (9) and re-expressing the surface density as a function of the impact parameter b, we find

$$\Sigma(x, \beta) \longrightarrow D \times (M_{200})^{\frac{\beta+1}{3}} \frac{f(c)}{c^{\beta-2}} \rho_c^{\frac{2-\beta}{3}} \frac{1}{b^\beta} \qquad \text{for } x \gg 1, \tag{11}$$

where D is a numeric constant of the order of unity. We see from the above that, as expected, $\Sigma \propto b^{-\beta}$, but in the pre-factors, there is a degeneracy between the mass of the halo M_{200} and a function of the concentration parameter c in the large x limit.

Hence, for a given fixed slope β, a heavy but high concentration halo will magnify to the same extent as a lighter, less concentrated halo. We will therefore find it useful to adopt a model for c.

2.2.1 *Concentration models*

In the original paper of Navarro et al. (1996), the NFW halo was characterized as a one-parameter family where $c \equiv c(M_{200})$. Recent studies have updated this result. Duffy et al. (2008, hereafter D08) used *Wilkinson Microwave Anisotropy Probe* (*WMAP*)-derived cosmological parameters to simulate haloes in the mass range 10^{11}–$10^{15}\, h^{-1}\,\mathrm{M}_\odot$, fitting

$$c = A(M_{200}/M_\star)^B (1+z)^C \ , \tag{12}$$

where $A = 5.71 \pm 0.12$, $B = -0.084 \pm 0.006$, and $C = -0.47 \pm 0.04$. Muñoz-Cuartas et al. (2011, hereafter MC11) also use a *WMAP*-derived cosmology with similar resolution and fit

$$\log c = a(z) \log M_{200}/[h^{-1}\,\mathrm{M}_\odot] + b(z) \tag{13}$$

$$a(z) = wz - m \tag{14}$$

$$b(z) = \frac{\alpha}{(z+\gamma)} + \frac{\beta}{(z+\gamma)^2} \ , \tag{15}$$

where $w = 0.029$, $m = 0.097$, $\alpha = -110.001$, $\beta = 2469.72$, and $\gamma = 16.885$. Finally, Mandelbaum, Seljak & Hirata (2008, hereafter M08) compile weak-lensing analyses of SDSS galaxies in the mass range 10^{12}–$10^{14}\, h^{-1}\,\mathrm{M}_\odot$ and fit

$$c = \frac{c_0}{(1+z)} \left(\frac{M}{M_\star}\right)^{-\beta} \ , \tag{16}$$

where $c_0 = 4.6 \pm 0.7$, $\beta = 0.13 \pm 0.07$, and $M_\star = 1.56 \pm 0.12 \times 10^{14}\, h^{-1}\, \mathrm{M}_\odot$.

For our data, we find $\langle c \rangle = 5.2$, 8.0, and 6.9 for the D08, MC11, and M08 models, respectively. We test our results on all concentration models, and also c as a uniform global parameter for comparative purposes. For our main result, we will prefer the M08 model as it has been derived from observations.

2.3 Homogeneous cosmology

For our background cosmology, we assume a spatially flat ΛCDM model, and neglect Ω_r so that $\Omega_\Lambda = 1 - \Omega_\mathrm{m}$. We have for the angular diameter distance D_A and luminosity distance D_L the standard formulae

$$\begin{aligned} D_\mathrm{L}(z) &= \frac{c}{H_0}(1+z_\mathrm{obs}) \int_0^{z_\mathrm{cos}} \frac{\mathrm{d}z'}{E(z')}\,, \\ D_\mathrm{A}(z) &= D_\mathrm{L}/(1+z_\mathrm{obs})^2, \\ E(z) &= \sqrt{\Omega_{\mathrm{m},0}(1+z_\mathrm{cos})^3 + \Omega_\Lambda, 0}\,, \end{aligned} \tag{17}$$

where H_0 is the present-day Hubble constant, $H(z) = H_0 E(z)$, and $\Omega_{\mathrm{i},0}$ is the present-day component density. z_obs refers to the observed heliocentric redshift, and z_cos the redshift corrected for peculiar velocity to the CMB rest frame. When using standard candles, it is convenient to re-express the luminosity distance as the distance modulus

$$\mu(z) = 5 \log_{10}(D_\mathrm{L}(z)/10\,\mathrm{pc})\,. \tag{18}$$

Our results depend only very weakly on the cosmological parameters used (via the angular diameter distances used in Σ_crit, and ρ_c used to normalize the halo density), except in the case of the physical mass-to-light ratio. However, to be concrete, we set $h = 0.674$ and $\Omega_\mathrm{m} = 0.298$, where $H_0 = 100\,h\,\mathrm{km\,s^{-1}\,Mpc^{-1}}$ and Ω_m is the best fit to the Pantheon sample.

2.4 Density model

Our model for the matter density is

$$\rho(\boldsymbol{r}, z) = \rho_\mathrm{void}(z) + \sum \rho_\mathrm{halo}(\boldsymbol{r}, \boldsymbol{r}_i, z), \tag{19}$$

where $\rho_\mathrm{halo}(\boldsymbol{r}, \boldsymbol{r}_i, z)$ is the density profile of a dark matter halo located at $\boldsymbol{r}_i$ and redshift z. $\rho_\mathrm{void}(z)$ is a spatially uniform minimum density that is a function of redshift only; it represents the average remaining density of the universe if the virial masses of galactic haloes were removed, and is determined by the requirement that $\bar{\rho} = \rho_\mathrm{c}$. We take the form of these haloes to be the spherically symmetric profiles as described in the previous section. Although we can in general expect the haloes to be non-spherical, it has been shown that after taking the average over randomly oriented non-spherical haloes for a lensing calculation, spherical symmetry is a very good approximation (Mandelbaum et al. 2005). We neglect additional inhomogeneous contributions due to filaments or sheets, and assume that baryons are distributed with the same profile as dark matter for the purposes of a magnification calculation.

2.4.1 *Flux conservation*

It can be shown that in the weak-lensing approximation, the average magnification (over a large number of sources) compared to a homogeneous background is unity (see e.g. Kainulainen & Marra 2009). In fact, this argument, which was originally made in a more general context by Weinberg (1976), depends on three key assumptions. First, the universe is assumed to be transparent and LOSs are not 'special' in some way. [Weinberg argued that if galaxies are opaque discs, and hence the LOSs are those that are unobscured by foreground galaxies, the average result will be de-magnification; Kainulainen & Marra (2011a) give a quantitative prescription for calculating this effect in terms of a survival probability as a function of impact parameter.] Secondly, the distance of sources is unaffected by lensing, which introduces perturbations to the sphere of constant redshift. Kaiser & Peacock (2016) have shown that this is equivalent to working to first order in the convergence κ. Thirdly, by working to first order in post-Newtonian potential Φ, the 'back reaction' of inhomogeneity on space–time is neglected and it is assumed that the homogeneous universe formulae (17) may continue to be used. What may happen in the more general non-perturbative case is still the subject of active research (see e.g. Buchert et al. 2015).

Therefore, working to first order in the convergence,[2] we take

$$\langle \Sigma_j \delta m_{i,j} \rangle = 0\,, \tag{20}$$

where sum is over $j = 1 \ldots N_i$ foreground galaxies and the average is over $i = 1 \ldots N_k$ sources in the redshift bin $z \in (z_k, z_{k+1})$. For lensing by galactic haloes at $z < 1$, our typical calculated $\Delta m \equiv \Sigma_j \delta m$ are $\mathcal{O}(10^{-2})$ to $\mathcal{O}(10^{-3})$. We therefore expect equation (20) to be a good approximation at redshifts $z < 1$ for sources that are weakly lensed. However, were we to be analysing sources at redshift $z \sim 2$ with $\Delta m \sim \mathcal{O}(10^{-1})$, second-order effects should not be ignored.

3 DATA

3.1 Supernovae

SN Ia magnitudes are standardized by the Tripp estimator (Tripp & Branch 1999), which is a function of observable features of their light curves. A commonly used form expresses the distance moduli μ of an SN Ia as

$$\mu = m_B - M_B + \alpha x_1 - \beta c + \Delta_\mathrm{M} + \Delta_\mathrm{B}\,, \tag{21}$$

where the observables are m_B, the peak apparent AB magnitude of the supernova; x_1, the 'stretch' of its light curve (a dimensionless parameter typically between −2 and 2 representing the duration of the curve); and c, the deviation of the $B - V$ colour from the mean colour. M_B is the absolute magnitude of a fiducial mean SN Ia light curve. Δ_M is a correction based on the host galaxy mass or other environmental effects, and Δ_B is a bias correction derived from simulations to account for the selection process of the sample. The nuisance parameters α and β are fitted for to minimize residuals versus a background cosmology.

For this analysis, we use the Pantheon data set[3] (Scolnic et al. 2018). The file `ANCILLIARY_G10.FITRES` contains the apparent magnitudes (adjusted using equation 21), redshifts, positions, stretch x_1, and colour c of 1048 SN Ia compiled from multiple surveys, with bias corrections determined according to the intrinsic scatter model of Guy et al. (2010). We also use the covariance matrix

[2] It is the flux of photons that is conserved on average, not any non-linear quantity such as magnitude derived from it. However, the correction is second order and we neglect it.

[3] https://github.com/dscolnic/Pantheon

`sys_full_long.txt`. We select the 901 SN Ia within the SDSS footprint.

3.1.1 Field selection

To obtain a clean lensing signal, we must identify the host galaxy: The supernovae will not be lensed by its host halo. If we fail to identify the host, due to errors in galaxy redshifts (see below), the true host may be present in the foreground close to the LOS, and so add a large spurious amount to the lensing estimate. We identify the galaxy closest in angular distance to the location of the supernova as the host, and exclude it from our lensing estimator. We also check that the redshift of the putative host is compatible with the redshift of the SN Ia. A limitation of this is that the SDSS photometric redshift confidence intervals are not always reliable, so in our results section we also quote the correlation using angular distance only for comparison.

To check we have indeed correctly identified the host, we also calculate the impact parameter of the closest galaxy in units of galactic scale length $x = b/r_s$. Large values will indicate doubt that we have identified the correct host, and we discard fields with $x > 4$ (corresponding to 100 kpc for a typical galaxy). The cutoff for x should not be too small as to unnecessarily remove supernovae originating in faint nearby satellite galaxies or the stellar halo, but not extend past the virial radius $x \sim c$. This selection reduces the sample to 762 supernovae.

To reduce noise, we further exclude fields that are more than 50 per cent masked in the foreground galaxy sample, as the lensing estimate is unlikely to be accurate for them. 35 per cent of our fields have some masking in them, with the average fraction of masked objects in those fields ~ 20 per cent. Our final sample therefore comprises 720 SN Ia.

3.2 Galaxies

We use galaxies drawn from the SDSS (Eisenstein et al. 2011). The survey performed deep imaging of 8400 deg^2 of the high Galactic latitude sky, and spectroscopy of over 1.5 million galaxies. A supernova survey was conducted of the so-called Stripe 82, a strip 2.5 wide along the celestial equator from right ascension 20^h to 4^h, and this is a prominent overlap with the Pantheon footprint. The galaxy survey is expected to be 95 per cent complete at $r = 22.2$ mag limit (Abazajian et al. 2009), and the faintest sources categorized as galaxies are up to $r \sim 26$.

We initially select all photometric objects in the SDSS Data Release 16 view `Galaxy`, which are in an aperture of radius 8 arcmin around the LOS to each supernova. For redshift $z = 0.2$, this corresponds to a physical distance of $\sim$1.5 Mpc. We discuss and test the choice of aperture in Section 5. We find 728 280 galaxies, of which 176 872 are in the foreground of their supernovae. The average redshift of our foreground sample is $z \sim 0.34$. We select photometric data in the *gri* passbands, using the `cModelMag` magnitudes m_λ as the best representation of the brightness of galaxies.

We select galaxies with clean photometry identified by the flags `InsideMask`=0 and `Clean`=1, which reduces our sample size by 33 per cent. We derive the absolute magnitude M_λ of the galaxy in a given passband as

$$M_\lambda = m_\lambda - \mu(z_p) - K_\lambda - A_\lambda \ , \tag{22}$$

where the survey-reported K-corrections K_λ and Milky Way extinction A_λ are used. The distance modulus μ is derived using the photometric redshift z_p by equations (17) and (18). We floor M_λ at -25 to reduce outliers. Our sample is illustrated in Fig. 3.

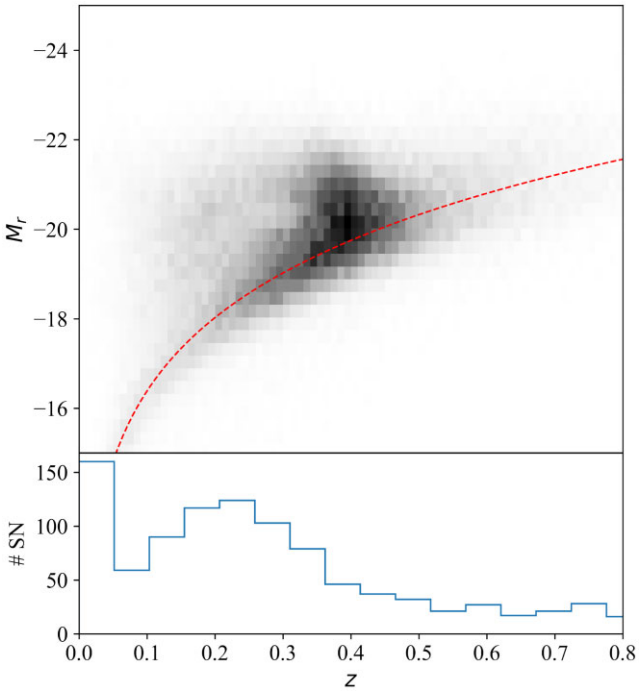

Figure 3. Number distribution of our galaxy and supernovae sample by calculated r-band absolute magnitude M_r and redshift z. The red dotted line shows the SDSS survey limiting magnitude $m_r = 22$, the effect of which is clear in the sample.

3.2.1 Photometric redshifts

We use the SDSS photometric redshifts z_p that were last updated in Data Release 12. The methodology used to determine them is outlined by Beck et al. (2016). The errors are calculated for each galaxy and are distributed as $\delta z_p \sim 0.09 \pm 0.04$, and the relative error $\delta z_p/(1 + z_p)$ is largely uncorrelated with redshift. The algorithm provides a flag `photoErrorClass` to indicate the quality of the fit, which is given as values between -7 and $+7$. There is some correlation between `photoErrorClass` and redshift, and to minimize selection bias, we therefore only exclude galaxies with `photoErrorClass` < -4, which is indicative of a poor-quality extrapolation from the training set.

For each galaxy j in the field of SN Ia i, we compute the angular diameter distances and impact parameter $b = \theta D_d$ using formulae (17), using the photometric galactic redshift z_p and the spectroscopic SN Ia redshift z. We also use z_p to determine the average matter density at the location of the galaxy $\rho_c(z) = 3H(z)^2/8\pi G$, which given the mass of the halo M_{200} will determine its physical radius r_{200} by equation (7).

We have already discussed that the lensing efficiency (equation 3) is relatively insensitive to redshift error near its peak. Whilst the average relative redshift error on the whole galaxy sample is $\sim$ 35 per cent, we find a relative error on the lensing efficiency of $\sim$ 20 per cent.

Our final sample then comprises 68 039 galaxies. Our selection parameters are summarized in Table 1, and in Section 5, we test the dependence of our results on these choices.

Table 1. Summary of parameter choices and selection criteria of foreground galaxies. See Section 2.5 for a description of the concentration models.

Parameter	Rationale	Value
Max radius	Include galaxies within an annulus (arcminutes)	8
`photoErrorClass`	Exclude galaxies with low-quality redshifts	-3 to $+7$
`InsideMask`	Exclude galaxies that are in masked areas	0
`Clean`	Exclude galaxies with poor photometry	1
Magnitude	Cap abs mag of galaxies to reduce outliers	-25
Concentration	Cap derived concentration to reduce outliers	15
Masked fraction	Exclude SN Ia with heavily masked foregrounds	50 per cent
Host radius	Exclude hostless SN Ia (within scale radii)	4
Concentration model	Degeneracy between halo mass and concentration	M08

4 METHODOLOGY

4.1 Estimating the lensing signal

We take dark matter haloes to be aligned to the photometric centre of individual galaxies. Hence, for magnification of supernovae i due to galaxy j, we set

$$\delta m_{i,j} \equiv \delta m(b_{ij}, \varpi_j), \tag{23}$$

where δm is given by equation (4). The impact parameter is $b_{ij} = \theta_{ij} D_{\mathrm{d},j}$, where θ_{ij} is the angular separation between galaxy j and supernova i and $D_{\mathrm{d},j}$ the angular diameter distance to the galaxy.

The halo parameters are $\varpi_j = \{M_{200,j}, c_j, \beta\}$. To estimate M_{200}, we convert the galactic absolute magnitude M_λ using a halo mass-to-light ratio Γ by

$$M_{200} = \Gamma(M_{200}, p) 10^{0.4(M_{\odot,\lambda} - M_\lambda)}, \tag{24}$$

where $M_{\odot,\lambda}$ is the solar absolute magnitude. $\Gamma(M_{200}, p)$ will in general depend on both M_{200} and galaxy type p (e.g. morphology or colour).

Previous weak-lensing shear studies have examined the relationship between mass-to-light ratios and luminosities, morphological type, or colour. Mandelbaum et al. (2006) derive a relation between the luminosity of *central* galaxy in a cluster and the *total* cluster mass of $M \propto L^2$, but this is not applicable for our model. Van Uitert et al. (2011) finds little dependence of Γ in the SDSS sample on luminosity for $L < 7 \times 10^{11} L_\odot$, but early-type galaxies are heavier (see table 2 and fig. 9 of that paper). Brimioulle et al. (2013) finds $\Gamma \propto L^{0.12 \pm 0.11}$ for galaxies from the Canada–France–Hawaii Telescope Legacy Survey, with red (defined as $B - V > 0.7$) galaxies being heavier than blue at the same luminosity.

We do not have morphological information p for most galaxies in our sample. Additionally, the size of our SN Ia sample is not sufficient to adequately constrain mass-to-light ratios for subsamples by colour or luminosity. Therefore, we adopt $\Gamma(M_{200}, p) \equiv \Gamma$ as a uniform sample average for our analysis.

Summing contributions of individual galaxies, we obtain the unnormalized magnification

$$\Delta m_i' = \sum_{j=1}^{N_i} \delta m_{i,j} \ , \tag{25}$$

where N_i is the number of foreground galaxies in the supernova field.

We impose the flux conservation of equation (20) and define our *magnification estimator* as

$$\Delta m_i = \Delta m_i' - \langle \Delta m_k'(z_i) \rangle \ . \tag{26}$$

In the second term, the average is taken over all supernovae i in the redshift bin $z_k < z_i < z_{k+1}$. Hence, by construction, $\langle \Delta m_i \rangle = 0$ in each bin (although our result for correlation does not depend on this). In practice, most LOSs do not pass very close to a foreground galaxy, and those supernovae will be mildly de-magnified. A smaller number will be magnified and hence the distribution of Δm_i is skewed with the median and mode positive.

4.1.1 *SN Ia colour*

The Spectral Adaptive Light-curve Template (SALT2) fitter for supernovae (Guy et al. 2007) outputs a colour parameter $c = (B - V) - \langle B - V \rangle$, which is the difference between the colour at peak B-band magnitude and the average for the training sample.[4] This may be interpreted as the sum of some intrinsic colour scatter, plus reddening $E(B - V)$. Some portion of this reddening will be due to the host galaxy, and some will be due to extinction by dust embedded in foreground galactic haloes. SN Ia magnitudes are de-reddened by the Tripp estimator (equation 21), which subtracts the reddening βc, where $\beta \sim 3$ is a fitted parameter consistent with $R_V = 3.1$.

However, we may estimate the amount of reddening due to dust in foreground galactic haloes in the following way. The combined effect of magnification and extinction is

$$F = F_0 \nu \mathrm{e}^{-\tau_\lambda} \ , \tag{27}$$

where $\nu = F_{\mathrm{lens}}/F_0$ is the lensing magnification factor, and τ_λ is the wavelength-dependent optical depth. In magnitudes, we obtain

$$\Delta m(\lambda) \simeq 1.08(\tau_\lambda - \Delta\nu) \ , \tag{28}$$

where $\Delta\nu = \nu - 1$. As lensing is achromatic, it follows that $E(B - V) \simeq 1.08(\Delta m(B) - \Delta m(V))$. Menard et al. (2010) investigated dust extinction in galactic haloes by correlating the colours and magnitudes of quasars in the range $1 < z < 2.5$ with the angular distance to SDSS foreground galaxies, finding that the visual band magnification is offset about 1/3 by extinction.

By using the dust-to-mass ratio $\Upsilon = 1.1 \times 10^{-5}$ derived in Ménard, Kilbinger & Scranton (2010) and a typical host galaxy dust mass opacity $\kappa_V = 1540\,\mathrm{m^2\,kg^{-1}}$ (Weingartner & Draine 2001), we estimate

$$\Delta c \simeq 0.01694\ \Sigma(r)\ \mathrm{mag}, \tag{29}$$

where $\Sigma(r)$ is the surface density of the galactic halo.

[4]The distinction between the NFW concentration parameter c and colour should be clear from the context.

4.1.2 SN Ia stretch

Supernovae have a finite size, and there will be some time delay (due to both the differential path-length and time dilation) between light arriving from opposite sides of the expanding photosphere. In principle, at least, this may result in some of the magnification being subtracted out as an increased stretch parameter x_1 of the light curve when the magnitude is standardized by the Tripp estimator (see equation 21). The differential time delay is proportional to the product of light traveltime across the ejecta and the deflection angle $\hat{\alpha}$ (which is the gradient of the time delay across the ray bundle). Thus, taking an ejecta velocity of $\sim 0.05c$, a light-curve duration of $\sim$30 d, and a deflection angle of 10^{-2} rad, the differential time delay will be roughly 30 min. However, this translates into a change in stretch parameter of only $\Delta x \sim 5 \times 10^{-3}$ (for the relation between x_1 and the duration of the light curve, see fig. 2 of Guy et al. 2007). Hence, the magnitude will be adjusted upwards by $\sim$0.001 mag for a typical value of $\alpha \sim 0.15$ in the Tripp estimator. This is less than 5 per cent of the calculated magnification for the same light deflection angle. We therefore ignore this effect.

4.2 Correlating with Hubble diagram residuals

We determined the SN Ia distance modulus residuals $\mu_{\rm res}$ by fitting a Hubble diagram to minimize

$$\chi^2 = \mu_{\rm res}^T \cdot \mathbf{C}^{-1} \cdot \mu_{\rm res} \ , \tag{30}$$

where $\mu_{\rm res} = \mu - \mu_{\rm model}$ and $\mu_{\rm model}(H_0, \Omega_{\rm m}, z)$ is given by equation (18), where μ is the apparent SN Ia distance modulus $\mu = m - M$.

$\mathbf{C}$ is the Pantheon covariance matrix (Scolnic et al. 2018), which is the sum of statistical and systematic errors $\mathbf{C} = \mathbf{C}^{\rm stat} + \mathbf{C}^{\rm sys}$. The statistical error matrix is diagonal with entries given by

$$C_{ii}^{\rm stat} = \sigma_N^2 + \sigma_{\rm Mass}^2 + \sigma_{\rm v-z}^2 + \sigma_{\rm lens}^2 + \sigma_{\rm int}^2 + \sigma_{\rm Bias}^2 \ , \tag{31}$$

where the largest term is the intrinsic SN Ia dispersion $\sigma_{\rm int} \sim 0.08$. The (Gaussian) term for the dispersion caused by lensing is $\sigma_{\rm lens}(z_i) = 0.055 z_i$, as estimated by Jönsson et al. (2010) (for details on the other terms, see section 3.2 of Scolnic et al. 2018). $\mathbf{C}^{\rm sys}$ is the covariance matrix induced by the training of the SALT2 model on a sample light-curve set.

Fitting was done using POLYCHORD (Handley, Hobson & Lasenby 2015), where we fix the SN Ia fiducial absolute magnitude $M = -19.43$, which is equivalent to setting $h = 0.674$. We find $\Omega_{\rm m} = 0.298 \pm 0.022$, consistent with Scolnic et al. (2018) (although our sample is a little smaller), and we use the central value to compute the residuals. The standard deviation of the residuals was $\sigma_{\rm res} \simeq 0.14$, which combines intrinsic, lensing, and all other sources of scatter.

We compute the bin k sample Pearson correlation coefficient ρ_k between $\mu_{\rm res}$ and Δm given in equation (26), which is

$$\rho_k = \frac{\sum_{z_i \in (z_k, z_{k+1})} (\mu_{i,\rm res} - \langle \mu_{\rm res} \rangle) \Delta m_i}{\sqrt{\sum (\mu_{i,\rm res} - \langle \mu_{\rm res} \rangle)^2} \sqrt{\sum \Delta m_i^2}} \ , \tag{32}$$

where the sum runs over all supernovae in bin k and $\langle \Delta m_i \rangle = 0$ in each bin by construction. We will also calculate the correlation of the colour parameter c and stretch x_1 with our lensing estimator Δm to check for dust extinction and any lensing time delay.

As an additional cross-check, we also obtain the *partial correlation coefficient* r_{ij} between variable i (i.e. Δm, $\mu_{\rm res}$, c, or x_1) and variable j. The partial correlation is defined as the Pearson correlation coefficient between the residuals of the two variables of interest when the others have been fitted out by linear regression. Setting $\Omega = (\rho_{ij})^{-1}$, it is given by

$$r_{ij} = -\frac{\Omega_{ij}}{\sqrt{\Omega_{ii}\Omega_{jj}}} \ . \tag{33}$$

4.3 Constraining halo parameters

We are additionally interested in deriving Bayesian posteriors for the halo model parameters ϖ. We use Bayes' theorem

$$P(\varpi | \boldsymbol{x}, \mathcal{M}) = \frac{\mathcal{L}_{\mathcal{M}}(\varpi) \pi_{\mathcal{M}}(\varpi)}{\mathcal{Z}_{\mathcal{M}}} \ , \tag{34}$$

where $\boldsymbol{x} = \mu_{\rm res} - \boldsymbol{\Delta m}$ is our data vector, and $\pi_{\mathcal{M}} = P(\varpi | \mathcal{M})$ is our prior belief in the parameters given the model $\mathcal{M}$. $\mathcal{Z}_{\mathcal{M}} = P(\boldsymbol{x} | \mathcal{M})$ is the evidence given by integrating the likelihood $\mathcal{L}_{\mathcal{M}} = P(\boldsymbol{x} | \varpi, \mathcal{M})$ over the prior, calculated as

$$\mathcal{Z}_{\mathcal{M}} = \int \mathcal{L}_{\mathcal{M}}(\varpi) \pi_{\mathcal{M}}(\varpi) {\rm d}\varpi \ . \tag{35}$$

We adopt the likelihood

$$\ln \mathcal{L} = \boldsymbol{x}^T (\mathbf{C}')^{-1} \boldsymbol{x}, \tag{36}$$

where the adjusted covariance $\mathbf{C}'$ is derived from the Pantheon covariance by removing the stated lensing variance:

$$\mathbf{C}' = \mathbf{C} - (0.055 z_i)^2 \ . \tag{37}$$

Although in principle extra variance from uncertainties in our lensing calculation should be included, they are relatively small compared to the intrinsic SN Ia residual variation, and we can neglect them. Indeed, we find that the distributional properties of $\boldsymbol{x}$ for our sample match this likelihood very well, with residual non-Gaussian properties being small.

We use uniform priors where the mass-to-light ratio $\Gamma \in (40, 400)$ and the halo radial profile slope $\beta \in (0.5, 4.0)$, and when extending to a variable uniform concentration, the halo concentration $c \in (2, 15)$. To derive our posteriors, we use the nested sampling method implemented in POLYCHORD (Handley et al. 2015).

5 RESULTS

5.1 Description of the lensing signal

In this subsection, we describe the features of the unnormalized magnification estimate given by equation (25), with the M08 concentration model and maximum-likelihood halo parameters (Γ, β) (see Eqn.1).

The majority of lensing signal comes from galaxies whose impact parameters lie within scale radius $x \simeq 5$–30. For a typical Milky Way-sized galaxy, this would be an impact parameter of $b \simeq 0.15$–1.0 Mpc. We illustrate this in Fig. 4. Comparing this to our profiles from Figs 1 and 2, we can see that we should be able to obtain moderate constraints on the slope parameter β, but that c is unlikely to be constrained very well by our sample.

In terms of which galaxies contribute to lensing, we show in Fig. 5 the aggregate estimate bucketed by galaxy absolute magnitude. Although the numbers of galaxies peak at $M \sim -20$, the lensing signal peaks at $M \sim -21.5$, which is equivalent to a Milky Way-type galaxy. In the plot, we have marked the absolute magnitude of an $m_r = 22$ galaxy located at $z = 0.25$, 0.4.

In Fig. 6, we show an illustration by redshift where the lensing estimate peaks. As expected, it is generally midway in redshift between the SN Ia and $z = 0$. For an SN Ia at $z \sim 0.5$ and a

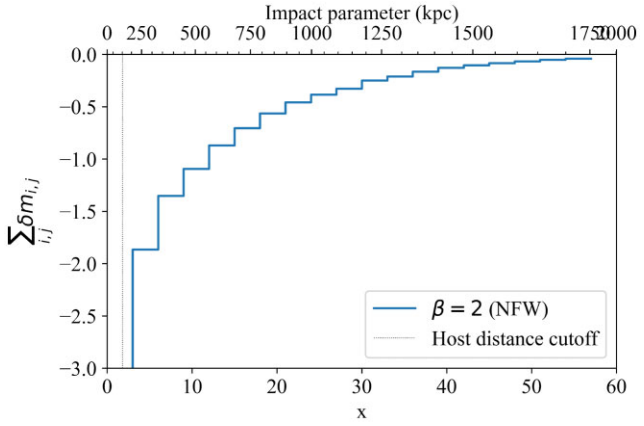

Figure 4. The aggregate unnormalized magnification of our sample, summed over all galaxies j and SN Ia hosts indexed by i. The lower axis is the impact parameter normalized to units of the scale radius $x = b/r_s$, where $r_s = r_{200}/c$. The upper axis is the impact parameter b averaged over the given x bin. Our host identification criteria of the projected distance of the SN Ia to the nearest galaxy in scale radii $x < 4$ are marked as a vertical black line at $r \sim 100$ kpc. Galaxies that are not SN Ia hosts will still contribute to our lensing calculation for $r < 100$ kpc.

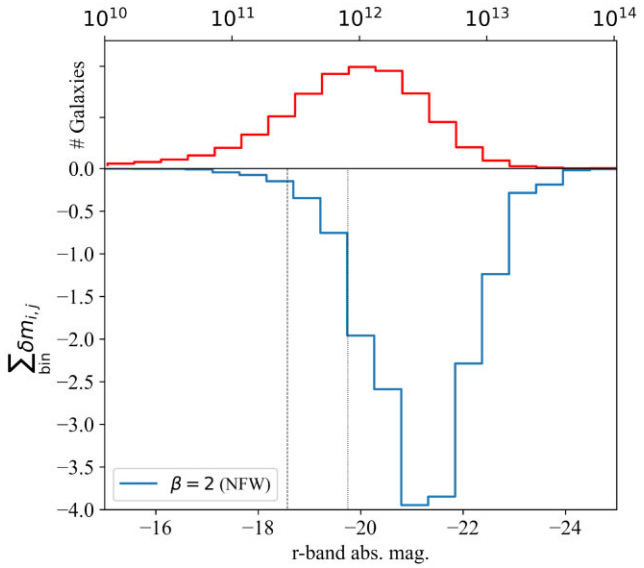

Figure 5. The upper panel shows the counts of galaxies in our sample binned by absolute magnitude M_r, with M_{200} shown on the upper x-axis in units of $M_\odot$. The lower panel shows our total lensing signal summed over galaxies and binned by absolute magnitude of the galaxy lens. The majority of our signal is within the SDSS limiting magnitude $m_r = 22$, marked for redshift $z = 0.25, 0.4$ as the vertical black dashed and dotted lines.

typical lensing galaxy at redshift $z \sim 0.25$, the magnitude limit $m_r = 22$ corresponds to $M_r = -18.5$, equivalent to the Large Magellanic Cloud (LMC). The mass of the LMC is ∼1/100 of a typical galaxy, and so galaxies below the survey limit at such intermediate redshifts will contribute a relatively small amount to the overall lensing signal, even taking into account their larger number density. However, for SN Ia at redshift $z \sim 1.0$, the typical lensing galaxy is $z \sim 0.4$ and so $M_r < -20.3$. We can now expect to be missing some fraction of the true lensing amount. We indeed see this in the top right-hand side of Fig. 6 as the reduced density of the lensing signal close to the diagonal line, compared to low and intermediate redshifts.

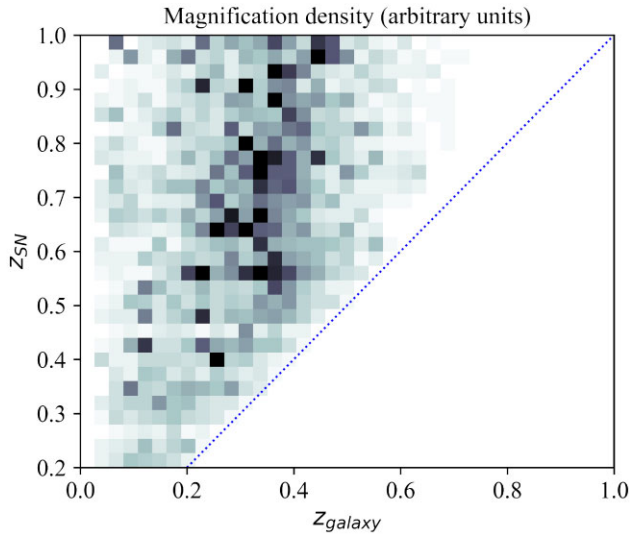

Figure 6. An illustration of the density of our lensing signal per SN Ia as a function of source redshift z_{SN} and lens redshift z_{galaxy}. Units are arbitrary, and are not shown. The lensing density peaks as expected, that is, roughly midway between the source and observer. The effect of the galaxy magnitude limit is to reduce the density in the upper right-hand corner of the plot.

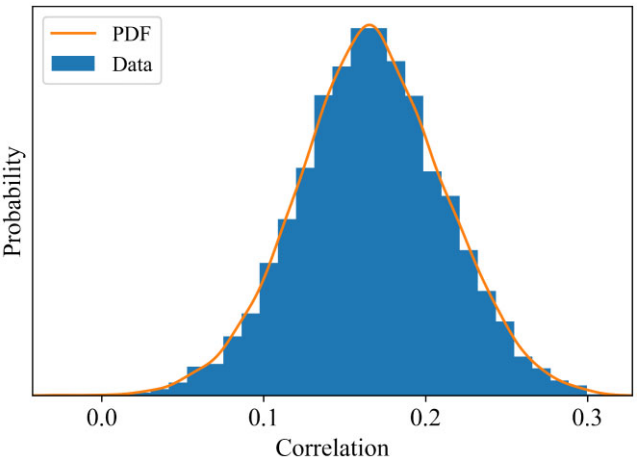

Figure 7. The bootstrap resampling distribution of correlation for our $0.2 < z < 1.0$ sample. The statistical significance of lensing signal detection obtained is $\bar{\rho}/\sigma_\rho = 3.6$.

5.2 Correlation of lensing estimate with SN Ia observables

For our best-fitting model, we find a correlation between our lensing estimate Δm and Hubble diagram residual μ_{res} of $\rho = 0.166 \pm 0.045$(stat) for SN Ia with $0.2 < z < 1.0$. This is a significance of 3.7σ before allowance for systematics.

The errors quoted have been derived from 10 000 bootstrap resamples of data (Fig. 7). It is clear we should exclude low-z SN Ia, as we do not expect them to be measurably lensed. We also exclude $z > 1$ SN Ia for several reasons. First, we expect them to be lensed to a significant degree by galaxies below the magnitude limit of the SDSS survey. Secondly, they are drawn from surveys conducted by the *Hubble Space Telescope* (*HST*; see e.g. Riess et al. 2007), so the targeting and detection efficiency may differ considerably from ground-based surveys. In any case, there are not enough numbers of them for this exclusion to affect our result. The result is not greatly

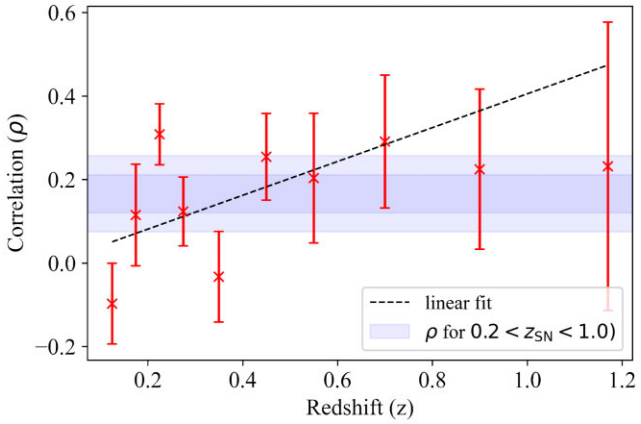

Figure 8. The correlation ρ between the Hubble diagram residuals and weak-lensing convergence estimate of our SN Ia sample, shown for individual redshift bins. Errors are computed by bootstrap resampling. The horizontal axis shows the average redshift in each bin. Our main result of $\rho = 0.166 \pm 0.046$ for the sample in the range $0.2 < z < 1.0$ is shown as the shaded purple bars at 1σ and 2σ confidence. As expected, for a signal due to lensing, we see a generally increasing trend with distance, and a linear fit to the correlation is marked. The trend towards larger error bars with increasing redshift is due to the smaller numbers of SN Ia in distant bins. Additionally, for the bins $z > 0.8$, the reduced significance is also due to the small angular field of the high-z *HST* surveys: There is not enough variation in the density of foreground galaxies across the field to show a correlation (this is discussed further in Section 5.5).

changed for other concentration models; for the D08 model, it is $\rho = 0.166 \pm 0.046$(stat), for MC11, it is $\rho = 0.166 \pm 0.046$(stat), and for a fixed $c = 6$, it is $\rho = 0.151 \pm 0.048$(stat).

Our other parameter choices were specified in Table 1. As expected, the correlation drops if we do not exclude SN Ia with poorly identified hosts: for no exclusions, $\rho \sim 0.11$. We discuss the dependence on other analysis parameter choices in the next subsection.

For the NFW profile, we find $\rho = 0.159 \pm 0.046$(stat), and for the SIS halo profile, $\rho = 0.149 \pm 0.046$(stat). The dependence of the SIS correlation on aperture radius is greater than for the NFW model, and as expected the correlation declines with wider aperture as remote field galaxies dilute the lensing signal. Anticipating the results from the full Bayesian analysis described in the next section, profiles close to NFW are likely to be preferred to those close to SIS. The result for the $\beta = 3$ Hernquist profile is $\rho = 0.097 \pm 0.046$(stat).

In Fig. 8, we show the correlation per redshift bin; as we would expect, we see a generally increasing trend with redshift, within the limitations of Poisson noise given ∼50 SN Ia per bin. We show scatter plots of our residuals in Fig. 9. As previously argued, the majority of our SN Ia are de-magnified and a smaller number of SN Ia are magnified. The intrinsic scatter dominates for low redshifts, but for larger redshifts, the correlation is visible in the grouping of dots towards the bottom left-hand and top right-hand quadrants. Our correlation is lowered by a few outliers, notably the SNLS supernovae 05D3hh, 04D3nr, 05D3km, 05D3mh, and 04D3gx, which are points well inside the upper left-hand quadrants in the bins $0.6 < z < 1.0$. These are SN Ia that have foreground galaxies close to the LOS but are dimmer than the Hubble diagram fit. Four out of five of these were originally classified by the survey as 'probable' (rather than certain; see Conley et al. 2011) SN Ia due to some ambiguity in their spectral classification. The proportion of probable SN Ia in the survey is ∼ 20 per cent, so it is possible that they represent contamination of the sample by non-SN Ia. Nevertheless, they have passed Pantheon quality cuts for their light-curve fitting, and there is no objective reason to exclude them. Without the additional criteria of compatibility of redshift between the host galaxy and SN Ia, the correlation is $\rho = 0.177 \pm 0.046$. Hence, the effect of the outliers is to modestly reduce the statistical significance from 3.9σ to 3.7σ.

The correlation of our lensing estimate with colour is not significant at $\rho_c = 0.024 \pm 0.05$. This result means we have no evidence for dust extinction in galactic haloes. This is consistent with Smith et al. (2014), who also found no correlation between colour and their lensing estimate, but does not contradict the results of Menard et al. (2010). The reason for this is that we find the average colour variation for our sample, as computed by equation (29), to be $\Delta c \sim 0.002$, whereas for magnification, our lensing signal is between 10 per cent and50 per cent of the intrinsic variation, and for colour our signal is just 2 per cent of the intrinsic variation of $\sigma_c \sim 0.1$. We would therefore only expect dust extinction to be detected only if we had a sample exceeding 10 000 SN Ia.

The correlation between lensing and stretch is not significant at $\rho_{x_1} = 0.047 \pm 0.047$ [in the literature, Smith et al. (2014) have reported a 2.2σ significance]. As a further test, we confirm that the partial correlation coefficients are consistent with our results.

We summarize our results on correlation in Tables 2 and 3.

5.2.1 *Correlation systematics*

We test the robustness of our results to our parameter choices; our correlation is unlikely to be overestimated by a 'bad' parameter choice, but we seek to estimate a systematic error to complement our statistical errors.

We perform the following tests on photometric selection criteria. We vary the passband used to calculate the absolute magnitude (and hence mass) of the lensing galaxies. We test the effect of varying the magnitude limit for galaxies above and below the formal survey limit at $m_r = 22$. As we would expect, if we adopt a lower limit, we exclude some galaxies that would contribute to the lensing signal, and the correlation drops. We additionally test the effect of varying our criteria for accepting heavily masked fields. If this selection parameter is too low, we drop too many SN Ia and the correlation drops. Alternatively, adopting too many masked fields adds noise to the signal and again the correlation drops. We find that our chosen cut of 50 per cent works well.

Photo-z errors will affect all physical distances used in our calculation, including angular diameter distances, the impact parameter $b = D_d(z)\theta$, and the critical surface density $\Sigma_c(z)$. As the convergence $\kappa \propto 1/b^\beta$, it is immediately clear that a bias might be introduced into our lensing calculation, even if the underlying photometric redshifts are themselves unbiased. In particular, the steeper the halo profile, the larger the potential bias. Further, it is likely that photo-z errors will be correlated to some degree (given the size of the training set relative to the survey size), but the degree of such covariance is difficult to estimate.

We address photo-z errors by multiplying each z by a random lognormal error of width $\sigma_z/(1 + z)$, and rerunning our analysis. We also test the relatively extreme scenario of always multiplying or dividing by the relative error – this is intended to determine the effect of fully correlated errors in redshifts. We additionally test the exclusion criteria for poor-quality redshifts by varying the maximum and minimum photo-z error class we select.

Adopting the average of the change in our correlation across our choices as an estimate of potential systematics, we find $\sigma_\rho =$

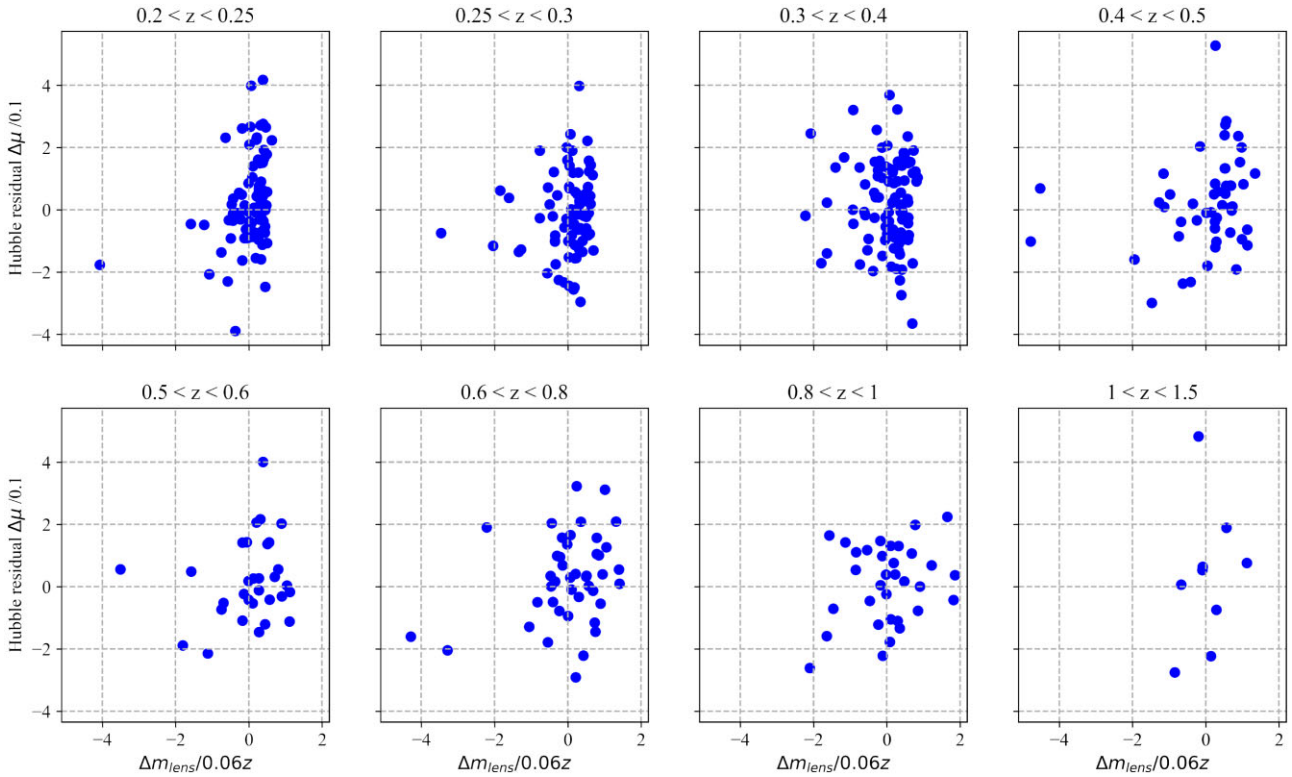

Figure 9. Scatter plots of Hubble diagram residuals $\mu_{\rm res} = \mu - \mu_{\rm model}$ of SN Ia (y-axis) and the lensing estimate Δm (x-axis). We have normalized the scales by dividing by the expected dispersion $\sigma_{\rm lens} = 0.06z$ and intrinsic dispersion $\sigma_{\rm int} = 0.1$. For low-redshift bins, we see the intrinsic dispersion of magnitudes, which has low skew and $\sigma_{\rm int} \sim 0.1$. For higher redshift bins, the correlation is apparent as the clustering of points in the top right-hand quadrant (the majority of LOSs are through underdense regions) and a small number of magnified supernovae in the bottom left-hand quadrant. A small number of outliers are present; in particular, in the $0.6 < z < 0.8$ bin, the point in the top left-hand quadrant is SN 05D3hh (see text for comment).

Table 2. Pearson correlation coefficient between the lensing signal Δm, SN Ia Hubble diagram residual $\mu_{\rm res}$, colour c, and stretch x_1. The significance of each correlation (including systematics) is also given in parentheses. Our main result is highlighted in bold.

	c	x_1	Δm
$\mu_{\rm res}$	−0.020(0.3)	−0.027(0.5)	**0.166(3.6)**
c	–	0.025(0.5)	0.024(0.5)
x_1	–	–	0.047(1.0)

Table 3. Partial correlation coefficient between the lensing signal Δm, SN Ia Hubble diagram residual $\mu_{\rm res}$, colour c, and stretch x_1. The results are largely unchanged compared to the Pearson correlation.

	c	x_1	Δm
$\mu_{\rm res}$	−0.023	−0.035	0.168
c	–	0.024	0.026
x_1	–	–	0.051

0.011(sys). Adding this in quadrature to our statistical error gives our main result $\rho = 0.166 \pm 0.046$ (stat + sys). This is a detection significance of 3.6σ.

5.3 Halo parameters

We find for the M08 model mean values of $\beta = 1.8 \pm 0.3$ and $\Gamma = 197^{+64}_{-80}\, h\, {\rm M}_\odot\, L^{-1}_{r,\odot}$ where marginalized 65 per cent confidence intervals are indicated.[5] The posteriors on our model parameters imply an additional error on ρ of $\sigma_\rho = 0.007$(post). For comparison, the maximum-likelihood values are $\beta = 1.7$ and $\Gamma = 196\, h\, {\rm M}_\odot\, L^{-1}_{r,\odot}$. Fixing $\beta = 2$, the NFW profile gives $\Gamma = 224^{+58}_{-79}\, h\, {\rm M}_\odot\, L^{-1}_{r,\odot}$.

We find that our results are again largely unaffected by the choice of concentration model; the D08 model prefers a slightly higher β as its average concentration is lower than M08, and conversely the MC11 model prefers a lower β for the same reason.

We find for the power-law model that $\beta > 1.2$ at 95 per cent confidence regardless of the concentration model used, and thus $\beta = 1$ (the modified SIS profile) is disfavoured to high confidence. We are also able to rule out the Hernquist profile at > 95 per cent confidence. The posteriors are illustrated in Fig. 10. As discussed in Section 2 in the context of concentration, we see some degeneracy between β and Γ, whereby a higher β favours more massive haloes to produce equivalent lensing power.

We test the effect of allowing a (uniform) c to vary globally across our galaxy sample. For the NFW model, we find $c = 4.3^{+1.0}_{-2.0}$. This value is consistent with our concentration models above. We also test running a loosely constrained model where all of (Γ, β, c) are allowed to vary. In this case, we find marginal values of $\Gamma = 185^{+55}_{-80}\, h\, {\rm M}_\odot\, L^{-1}_{r,\odot}$, $\beta = 1.8^{+0.2}_{-0.6}$, and $c = 7.5^{+6.3}_{-5.3}$. These values are consistent with our main result above, although of course the confidence intervals are wider.

[5] We have re-introduced $h = 0.674$ to normalize our result here.

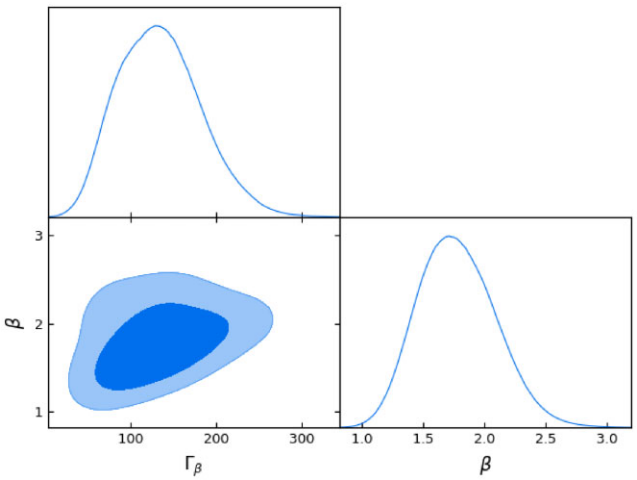

Figure 10. The derived posteriors for our power-law halo profile slope β and mass-to-light ratio Γ_β. $\beta = 2$ corresponds to the NFW profile. We also show the correlation posterior implied by the range of halo profiles; our core result of lensing detection is largely insensitive to the details of the profile. As explained earlier, there is some degeneracy between concentration determined by either β or c, and Γ_β: A more concentrated halo profile requires a higher mass to produce the same amount of magnification.

As a check to derive pieces of evidence for model comparison, we also run the SIS profile and derive a posterior for $\Gamma = 70^{+4}_{-11}\, h\, \mathrm{M}_\odot\, L^{-1}_{r,\odot}$.

The results for our runs are presented in Table 4. Comparing the Bayesian evidence, we find little preference between our different concentration models (first four lines). The SIS and NFW models are somewhat disfavoured compared to allowing a variable slope; to a certain extent, this is due to the presence of the small number of outliers (see Fig. 9), otherwise we would find β aligned with the NFW model.

5.4 Malmquist bias

Both our galaxy and supernova surveys are magnitude-limited, and and we estimate its effect on our results here.

The effect of the magnitude limitation $m_{\rm gal}$ of the galaxy survey is straightforward to understand. An SN Ia will be lensed by all galaxies along the LOS, whether seen or unseen. The redshift of a given SN Ia defines a volume limit applicable to foreground galaxies. Then, for SN Ia surveys paired with galaxy surveys on similar platforms, we will observe all contributing galaxies brighter than the SN Ia (and generally better than that, if the galaxy survey is deeper). Hence, we will be largely unaffected by the galaxy survey limit. However, the SNLS and *HST* surveys are deeper than SDSS, and we will underestimate the number of galaxies contributing to lensing. Hence, the signal-to-noise ratio and correlation will be lower, and the mass of low-z galaxies (i.e. the surface density attributed to them) will be overestimated.

The effect of the magnitude limitation $m_{\rm l}$ of our supernova survey is more complex. For a magnitude-limited sample, a small number of sources that would have been too faint to be seen in a homogeneous universe will magnify into the observed sample (and will be identified as overluminous SN Ia by their redshifts). Conversely, along underdense LOSs, SN Ia that are close to the magnitude limit will drop out of our sample. Taking the magnified SN Ia in isolation, flux conservation no longer holds: They represent overdense LOSs not representative of the homogeneous average. As their brightnesses sample the high-magnification tail of the lensing distribution, they will also show a greater dispersion. Hence, we can expect to see a spike in the dispersion of magnitudes in the redshift bucket containing $z(m_{\rm l})$ of the SN Ia sample.

A practical difficulty for SN Ia is that $m_{\rm l}$ is not well defined. The Pantheon compilation merges surveys with different limiting magnitudes. Further, only a small proportion of candidate supernovae (sometimes as little as 1 in 100) are targeted for a spectroscopic follow-up, and the transient nature of the source means the decision-making process may be influenced by many factors such as instrument availability, local seeing conditions, SN Ia environment, and so on, as well as magnitude. Hence, there is no $m_{\rm l}$, but instead a *detection efficiency* $f \in (0, 1)$ is defined as the ratio of SN Ia that will be in the spectroscopically selected sample, compared to one with no selection. f is determined by a model of the targeting algorithm and intrinsic scatter, and is thought to be well characterized by the observed magnitude m such that $f = f(m)$ (see e.g. the discussion in section 3.3 and fig. 6 of Scolnic et al. 2018). However, if a preference for a 'clean' LOS influences the selection, a sample biased towards underdense LOSs will result.

Taking the limits as where the survey is ~ 50 per cent complete, we set $m_{\rm gal} = 22.5$, $m_{\rm SDSS} = 22.5$, $m_{\rm PS1} = 23.0$, and $m_{\rm SNLS} = 24.3$ (we will not use *HST* data for reasons discussed in the next subsection). Interestingly, in Pantheon, the average stretch and colour parameters $\bar{c}, \bar{x_1}$ drift with higher redshift towards brighter SN Ia, and are most different from their mean of zero for the sharply truncated SNLS survey (see fig. 10 of Scolnic et al. 2018). If this is due to selection bias, it is probable that lensing will have a similar effect (however,

Table 4. A summary of the marginalized mean values and confidence intervals for Γ, β, and c, for a range of models and fixed or free parameters. Conc. refers to the concentration model used. Γ is in physical units of $\mathrm{M}_\odot\, L_{r,\odot}{}^{-1}$, but is not normalized by h here. log $\mathcal{Z}$ is the log of the mean likelihood as output by POLYCHORD. The first three rows correspond to different concentration models. The fourth row shows the result when $c = 6$ fixed – as this lower than is preferred in the free fit shown in the fifth row, so Γ is pushed high as a result. The sixth to ninth rows show Γ when the profile and concentration model are fixed. The last row shows a 'global' result where all parameters are allowed to vary, and is shown as a consistency check. Priors were $\Gamma \in (40, 400)$ and $\beta \in (0.5, 4.0)$, and when extending to a variable fixed concentration, $c \in (2, 15)$.

Profile	Conc.	Γ	65 per cent	95 per cent	β	65 per cent	95 per cent	c	65 per cent	95 per cent	log $\mathcal{Z}$	65 per cent
Power law	M08	133	79/176	46/229	1.8	1.4/2.1	1.2/2.4	–	–	–	688.3	0.2
Power law	D08	140	84/185	51/238	1.9	1.6/2.2	1.2/2.6	–	–	–	688.6	0.2
Power law	MC11	121	72/158	41/209	1.7	1.4/1.9	1.2/2.2	–	–	–	688.4	0.3
Power law	Fixed	164	50/211	36/355	2.1	1.6/2.4	1.4/3.1	6	–	–	688.9	0.2
NFW	Fixed	134	85/177	49/228	2	–	–	4.3	2.3/5.2	1.6/8.4	688.3	0.2
SIS	–	47	40/50	38/65	–	–	–	–	–	–	689.5	0.3
NFW	M08	151	98/190	64/249	2	–	–	–	–	–	689.3	0.1
Power law	Fixed	125	71/162	38/227	1.8	1.3/2.0	1.1/2.7	7.5	2.2/13.8	1.8/14.6	688.6	0.2

the drift might instead be attributed to population evolution at higher redshift; Nicolas et al. 2021).

We tested the effect of these magnitude limits using the pencil-beam light-cones of Henriques et al. (2012), which are magnitude complete to $z \sim 1$, derived from the Millennium Simulation (Springel et al. 2005; Lemson & Virgo Consortium 2006; Guo et al. 2010), and sourced from the German Astrophysical Virtual Observatory.[6] As a cross-check, we also used the broader MICE-Grand Challenge Galaxy and Halo Light-cone Catalog (Micecatv2.0), which is complete to $i < 24$ (Carretero et al. 2015; Crocce et al. 2015; Fosalba et al. 2015a,b; Hoffmann et al. 2015), sourced from CosmoHub[7] (Carretero et al. 2017; Tallada et al. 2020).

Using random LOSs and a fiducial $\Gamma = 150$, we examined the effect of imposing galaxy magnitude limits. The effect was to raise Γ by 15 per cent (SNLS), 5 per cent (PS1), and negligible change for the SDSS SN Ia survey. As a further test of the galaxy magnitude limit, we reran POLYCHORD for Pantheon and SDSS real data restricted to redshift $0 < z < z_{\rm max}$ for $z_{\rm max}$ between 0.5 and 1.0. This transitions our data sample towards (but not fully) volume-limited rather than magnitude-limited. We found a modest drift upwards in the maximum-likelihood Γ for lower $z_{\rm max}$, by about 8 per cent for $z_{\rm max} = 0.5$. This is consistent with the results from simulations above.

We next tested the effect of imposing the SN Ia survey limit. The dispersion of lensing was increased in the redshift bucket including the survey limit. As a result of the bias to overdense LOSs, Γ was lowered by about 15 per cent for SDSS, 5 per cent for PS1, and unchanged for SNLS.

Hence, the combined effect of the SN Ia and galaxy magnitude limits is somewhat offsetting in our data. By appropriately weighting the biases according to the number counts of each survey, we find that Malmquist bias is expected to be < 10 per cent on our derived parameters, well within the 1σ confidence intervals for the parameters we derive. We therefore do not adjust our fits.

5.5 Lensing dispersion

We present the dispersion of lensing for the $\beta = 1.8$ model with M08 concentration and mean $\Gamma = 133\,{\rm M}_\odot\,L_{r,\odot}^{-1}$ in Fig. 11. At redshifts $z > 0.8$, the dispersion starts to drop below trend as expected due to magnitude limits. We also show the dispersion for the $1 < z < 1.5$ bucket, which seems anomalously low. We only have nine SN Ia that pass our quality criteria in the bucket $1.0 < z < 1.5$, and all are from the *HST* surveys GOODS, CANDELS, and CLASH. There is a straightforward explanation: These were pencil-beam surveys, and most of the SN Ia are within a few arcminutes of each other. There will then be little variation between LOSs!

The standard deviation is sensitive to the high-magnification tail. Jönsson et al. (2010) argued that due to Poisson noise and the limited size of their sample (175 SN Ia), they were missing highly magnified $\Delta m < -0.25$ supernovae that would increase the dispersion. The authors replaced the dispersion from their actual sample $\sigma_{\rm lens} = 0.035z$ with $\sigma_{\rm lens} = 0.055z$, which was the dispersion from their best-fitting model across a large number of randomly selected LOSs. We are less likely to be affected by Poisson noise as we have higher numbers of SN Ia; Fig. 9 shows that there are adequate numbers of SN Ia with $\Delta m < -0.25$ for $z < 0.8$ but less so for the last two buckets. We therefore restrict our fit to $z < 0.8$ where the bias is small.

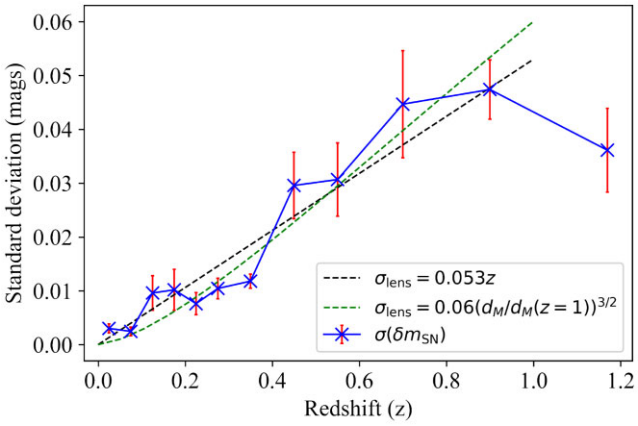

Figure 11. The dispersion of SN Ia magnitudes due to lensing. The error bars have been computed by bootstrap resampling. For $z < 0.8$, we estimate $\sigma_{\rm lens} = 0.053z$. This does not extrapolate well, and we introduce the new fit $\sigma_{\rm lens} = 0.06(d_C(z)/d_C(z=1))^{3/2}$, which is better motivated. The outlier in the $1 < z < 1.5$ bucket is due to the limited numbers of SN Ia in this bucket being within a few arcminutes of each other.

It is usual to fit for $\sigma_{\rm lens} = Az$, perhaps because the data appear visually linear. If we do so, we find $A = 0.053 \pm 0.015$. This is consistent with Jönsson et al. (2010), and also with Bergström et al. (2000), who found $\sigma_{\rm lens} = 0.04z$, but lower than Holz & Linder (2005), who estimated $\sigma_{\rm lens} = 0.088z$, both from simulations.

Obviously, this fit has a limited range, and extrapolating it beyond $z > 1$ is dubious. In Appendix B, we show that in the case of no clustering of galaxies,[8] a better fit is provided by

$$\sigma_{\rm lens} = B(d_C(z)/d_C(z=1))^{3/2}, \tag{38}$$

where we have normalized to the comoving distance at $z = 1$, and $d_C(z=1) = 3400\,{\rm Mpc}$ for our fiducial cosmology. We find $B = 0.06 \pm 0.017$ and the fit is shown in Fig. 11. This is likely to be a *lower bound* on the true dispersion, due to both the magnitude limitation of the survey and the effect of clustering (which introduces extra covariance between sources and lensing galaxies). We recommend to use this in cosmological parameter estimation, as it is generally higher than previously assumed values.

As a cross-check, we simulated 10 000 LOSs from randomly selected galaxies in the SDSS footprint, and recomputed the lensing variance. We did not find any significant difference from the above, and therefore conclude that our fit is unaffected by shot noise.

5.6 Comparison with shear studies

Direct comparisons of the mass-to-light ratio we derive to the literature are complicated by the selection of which luminosity to compare to which mass, and also differing halo profiles and truncations. For example, the comparison may be between the luminosity of the single brightest galaxy in a cluster and the mass of the entire cluster.

Regarding the radial dependence of the convergence, Menard et al. (2010) studied the magnification of quasars by galaxies drawn from the SDSS survey, finding the projected $\Sigma(r) \propto r^{-0.8}$ from 10 kpc to 10 Mpc. This is consistent with other shear studies (see e.g. Sheldon et al.

[6] http://gavo.mpa-garching.mpg.de/Millennium/
[7] https://cosmohub.pic.es/home

[8] This is equivalent to the 'stochastic' approaches of authors such as Holz & Linder (2005), Jönsson et al. (2010), and Marra et al. (2013).

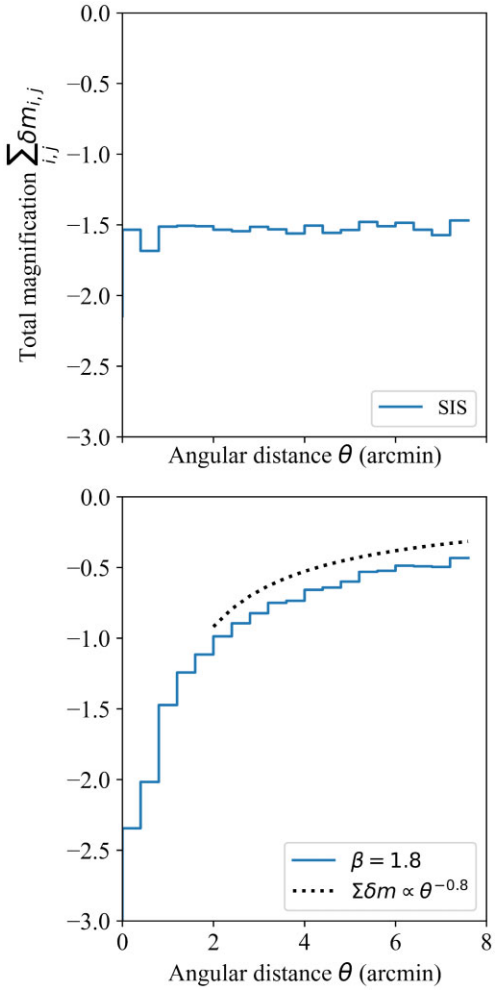

Figure 12. Our total lensing signal summed over galaxies and binned by angular distance θ from the SN Ia host. In the upper plot, we show the SIS halo calculation. We obtain a flat profile for the lensing signal as a function of angular separation because the increase in the numbers of galaxies within each increasing size of annulus of sets the lower surface density with larger separation. In the lower plot, we show the best-fitting $\beta = 2.14$ profile. In this case, the lensing signal is well fitted by θ^{-1}, which is consistent with shear studies.

2004). We find that after stacking our lensing estimate into angular buckets, the power-law model with $\beta = 1.8$ fits $\Sigma(\theta) \propto \theta^{-0.8}$. This is shown in Fig. 12. This is because a SIS profile for a total surface density surrounding a fiducial galaxy is mimicked by the overlapping contributions of nearby NFW haloes. For luminous red galaxies from the SDSS survey, Mandelbaum et al. (2006) found the NFW profile was preferred to the SIS at a confidence level of 96 per cent, and found an average $c = 5.3 \pm 1.2$.

There is good evidence that mass-to-light ratios depend on galactic morphology and colour. The value we derive here should be seen as a population average, weighted by luminosity. In a shear study, Van Uitert et al. (2011) compare the total luminosity within $r < r_{200}$ to the mass M_{200} for an NFW profile with the D08 concentration model. For bright early-type galaxies with $L > 5 \times 10^{11}\,L_\odot$, they find $\Gamma \sim 260\,h\,\mathrm{M}_\odot\,L_{r,\odot}^{-1}$, but considerably lower values for late-types or lower luminosities. In a galaxy–galaxy lensing study, Brimioulle et al. (2013) find $\Gamma = 178^{+22}_{-19}\,h\,\mathrm{M}_\odot\,L_{r,\odot}^{-1}$ at a reference luminosity of $L_r = 1.6 \times 10^{10}\,h^{-2}\,L_{r,\odot}$.

We may also compare our value to a 'cosmic' mass-to-light ratio; that is to say the value approached on large scales. Bahcall & Kulier (2014) examine shear around SDSS clusters and derive a cosmic $\Gamma = 409 \pm 23\,h\,\mathrm{M}_\odot\,L_\odot^{-1}$ (which is equivalent to $\Omega_\mathrm{m} = 0.26 \pm 0.02$). The authors state that the lensing signal of the entire cluster can be replicated by the sum of the contributions from individual galactic haloes; that is, there is no additional cluster dark matter beyond that centred on galaxies, as we have assumed in our model. It is interesting to note that this result in combination with ours would imply that the matter fraction not virialized into haloes is $\rho_\mathrm{void}/\rho \sim 0.5$.

In summary, we find our results for power-law slope consistent with the literature, and the mass-to-light ratio consistent with the (albeit large) range of values quoted.

6 SUMMARY AND DISCUSSION

In this paper, we have developed an estimator (equation 26) for the weak-lensing convergence based on the astrometric properties of foreground galaxies. The key assumptions underlying the estimator are

(i) a matter density comprised of universal halo profiles superimposed on a homogeneous background,
(ii) the magnification is weak,
(iii) the LOSs to SN Ia are equivalent to a random sample, and
(iv) the masses of dark matter haloes may be estimated from galactic magnitudes using an average mass-to-light ratio.

We have demonstrated the effectiveness of the estimator by correlating it with SN Ia residuals to a best-fitting Hubble diagram. Using a $\beta = 1.8$ profile with the M08 concentration model, this is $\rho = 0.166 \pm 0.046(\mathrm{stat}) \pm 0.011(\mathrm{sys})$ for SN Ia with $0.2 < z < 1.0$. This is a detection significance of $>3\sigma$, which improves on previous results of $\sim 1.4\sigma$ (Jönsson et al. 2010; Smith et al. 2014; Macaulay et al. 2020). Our results are not greatly affected if the NFW profile is used, or the choice of concentration model or analysis parameters within reasonable bounds.

It is natural to ask why we find a greater significance of our detection than the previous literature. First, we have a four times larger sample of SN Ia than Jönsson et al. (2010), and our use of a smooth halo profile incorporating the well-established NFW profile may capture the true density profile better than a truncated isothermal sphere as used by those authors. Secondly, as we explained in Section 2, magnification is highly sensitive to chance encounters with a low impact parameter. Although Smith et al. (2014) have similar numbers of SN Ia to us, the lensing is estimated from the number counts of foreground galaxies only; in our method, it would be equivalent to setting $\beta = 0$ and each halo to the same mass. As we saw in Section 5, lower β has a lower correlation detection significance. While Macaulay et al. (2020) used just 196 SN Ia, better photometry from the DES platform assisted their analysis. Nevertheless, it may be challenging to use skew as a detection method.

Using Bayesian analysis, we find the mean $\beta = 1.8 \pm 0.3$ and $\Gamma = 197^{+64}_{-80}\,h\,\mathrm{M}_\odot\,L_{r,\odot}^{-1}$. The SIS halo profile is ruled out at > 95 per cent confidence. Comparing the Bayesian evidence of the power-law and NFW profiles, we find no significant difference between the two.

In our model, Γ and β are uniform parameters over our entire galaxy sample, which extends in the range $-17 < M_r < -24$. As there may be variation by colour, luminosity, morphology, and environment, they should be interpreted as a weighted population average, with the peak of weighting at $M_r \sim -21$.

We have considered the effects of Malmquist bias on our results. We show that due to magnitude limits in the SN Ia data, Γ is likely biased low by ~ 10 per cent. This is well within the confidence interval of our posterior, and so we do not adjust our results for this. We have also shown that the lensing dispersion is biased low in the longer redshift buckets $z > 0.8$ due to magnitude limits and the small footprint of the *HST* surveys used in Pantheon.

We show that the lensing dispersion is fitted by

$$\sigma_{\rm lens} = (0.06 \pm 0.017)(d_{\rm C}(z)/d_{\rm C}(z=1))^{3/2}\,, \tag{39}$$

which is consistent with the often cited $\sigma_{\rm lens} = (0.055 \pm 0.04)z$ (Jönsson et al. 2010) for $z < 0.8$ but starts to diverge higher for $z > 1.0$. We can compare this number to intrinsic scatter $\sigma_{\rm int}$, which is the variation in SN Ia absolute magnitude once the light curves are standardized for colour, stretch, bias, and environment (see equation 21). Scolnic et al. (2018) report that $\sigma_{\rm int} = 0.09$ for Pantheon. However, the scatter is largest for the older low-z survey, and lowest for the newest Pan-STARRS data. Early results from the DES and Foundation SN Ia surveys indicate the true $\sigma_{\rm int} \sim 0.07$ (Brout et al. 2019). Equation (39) therefore shows that lensing will match intrinsic scatter at $z \sim 1.2$, which is closer than previously estimated (Jönsson et al. 2010). As a result, cosmological parameter precision will be degraded in high-z surveys (Holz & Linder 2005 estimate by a factor of 3 at $z \sim 1.5$).

Based on the above, we propose that inference of cosmological parameters may be improved in high-z surveys by modifying the Tripp estimator to include a specific term to de-lens the magnitudes as follows:

$$\mu = m_B - M_B + \alpha x_1 - \beta c + \Delta_{\rm M} + \Delta_{\rm B} - \gamma \Delta m_{\rm lens}\,. \tag{40}$$

The estimator $\Delta m_{\rm lens}$ (which may be seen as an environmental variable analogous and comparable in size to the host mass correction $\Delta_{\rm M}$) is given by equation (26). Mean parameters given in Table 4 can be used with $\gamma = 1$.[9] Testing this, we find for the Pantheon sample that equation (40) improves the standard deviation of the Hubble diagram residuals by 0.005 mag for $z > 0.4$.

In addition to correcting magnitudes, SN Ia lensing may be used as a source of cosmological information in itself, and we will explore this in future work.

6.1 Future surveys

In this work, we used the Pantheon SN Ia compilation because of its uniform calibration, well-characterized bias corrections, and large overlap with the SDSS galaxy survey. However, the drawbacks are the lack of a single SN Ia detection efficiency function (due to Pantheon merging several surveys) and shallow SDSS photometry. This meant the Malmquist bias was not straightforward to estimate.

The Dark Energy Survey (DES Collaboration 2016) offers several advantages. The associated supernova survey is expected to catalogue a few thousand *photometrically* classified SN Ia, down to a deep field depth of $r < 25.5$ (Smith et al. 2020). As a result of photometric classification, the detection efficiency will be simpler to model and there is less risk of a biased selection of LOSs. In addition, the foreground galaxy catalogue will be of equivalent depth as the supernova survey, and as a result bias should be small and straightforward to calculate. DES data have been used to produce a map of lensing convergence derived from a weak-lensing shear analysis (Jeffrey et al. 2021), and it will be particularly interesting to compare such maps derived from shear to those derived from magnification.

The Rubin LSST Observatory, expected to commence survey operations in 2023 October, will reach approximately 2 mag deeper. It is expected to catalogue $\sim 10\,000$ SN Ia each year (Zhan & Tyson 2018) in the range $0.2 < z < 0.8$ in the southern sky. With these enlarged data sets, we anticipate improved luminosity, morphological and colour characterization of $\Gamma(M, p)$.

Looking at space missions, the *Roman Space Telescope* will conduct an SN Ia search as part of its galaxy survey mission. With an optimized survey strategy (Hounsell et al. 2018), it may discover $> 10\,000$ SN Ia out to $z \sim 2.5$ over the course of its mission. The fractional distance modulus uncertainty per $0.1z$ bin is expected to be 4×10^{-3} (a factor of 10 improvement on the Pantheon data set). With this high-precision data set, we would expect to detect lensing at $>15\sigma$ confidence. It will be particularly interesting to test the modified Tripp estimator we proposed in equation (40) on this data set.

[9] A similar modification was proposed by Smith et al. (2014) with an estimator based on spectroscopic-only galaxies. The authors find $\gamma \sim 4$, which is driven mainly by the ratio of the number density of spectroscopic galaxies to photometric ones. However, as the spectroscopic galaxy coverage may not be uniform across a given survey, this estimator seems less practical.

ACKNOWLEDGEMENTS

We thank Edward MacAulay, David Bacon, and Sunayana Bhargava for helpful discussions on this work. We also thank the referee for helpful comments that have improved the paper.

The Millennium Simulation data bases used in this paper and the web application providing online access to them were constructed as part of the activities of the German Astrophysical Virtual Observatory (GAVO). This work has also made use of CosmoHub. CosmoHub has been developed by the Port d'Informació Científica (PIC), maintained through a collaboration of the Institut de Física d'Altes Energies (IFAE) and the Centro de Investigaciones Energéticas, Medioambientales y Tecnológicas (CIEMAT) and the Institute of Space Sciences (CSIC & IEEC), and was partially funded by the 'Plan Estatal de Investigación Científica y Técnica y de Innovación' programme of the Spanish government.

OL and PL acknowledge support from an STFC Consolidated Grant ST/R000476/1, and PL acknowledges STFC Consolidated Grant ST/T000473/1.

DATA AVAILABILITY

Upon publication, code, figure scripts, and sample SQL queries will be made available at https://github.com/paulshah/SNLensing.

REFERENCES

Abazajian K. N. et al., 2009, ApJS, 182, 543
Bahcall N. A., Kulier A., 2014, MNRAS, 439, 2505
Bartelmann M., Schneider P., 2001, Phys. Rep., 340, 291
Beck R., Dobos L., Budavári T., Szalay A. S., Csabai I., 2016, MNRAS, 460, 1371
Bergström L., Goliath M., Goobar A., Mörtsell E., 2000, A&A, 358, 13
Brimioulle F., Seitz S., Lerchster M., Bender R., Snigula J., 2013, MNRAS, 432, 1046
Brout D. et al., 2019, ApJ, 874, 150
Buchert T. et al., 2015, Class. Quantum Gravity, 32, 215021
Carretero J., Castander F. J., Gaztañaga E., Crocce M., Fosalba P., 2015, MNRAS, 447, 646

Carretero J. et al., 2017, in Checchia P., Mezzetto M., Salente G., Doro M., Conti L., eds, Proc. European Physical Society Conference on High Energy Physics (EPS-HEP2017), p. 488
Conley A. et al., 2011, ApJS, 192, 1
Crocce M., Castander F. J., Gaztañaga E., Fosalba P., Carretero J., 2015, MNRAS, 453, 1513
DES Collaboration, 2016, MNRAS, 460, 1270
Duffy A. R., Schaye J., Kay S. T., Vecchia C. D., 2008, MNRAS, 390, 64 (D08)
Eisenstein D. J. et al., 2011, AJ, 142, 72
Falco E., Gorenstein M., Shapiro I., 1985, ApJ, 289, 1
Fosalba P., Gaztañaga E., Castander F. J., Crocce M., 2015a, MNRAS, 447, 1319
Fosalba P., Crocce M., Gaztañaga E., Castander F. J., 2015b, MNRAS, 448, 2987
Freedman W. L. et al., 2019, ApJ, 882, 34
Frieman J. A., 1997, Comments Astrophys. Space Phys., 18, 323
Giblin B. et al., 2021, A&A, 645, A105
Guo Q., White S., Li C., Boylan-Kolchin M., 2010, MNRAS, 404, 1111
Guy J. et al., 2007, A&A, 466, 11
Guy J. et al., 2010, A&A, 523, A7
Hada R., Futamase T., 2016, ApJ, 828, 112
Handley W. J., Hobson M. P., Lasenby A. N., 2015, MNRAS, 450, L61
Henriques B. M. B., White S. D. M., Lemson G., Thomas P. A., Guo Q., Marleau G.-D., Overzier R. A., 2012, MNRAS, 421, 2904
Hernquist L., 1990, ApJ, 356, 359
Hoffmann K., Bel J., Gaztañaga E., Crocce M., Fosalba P., Castander F. J., 2015, MNRAS, 447, 1724
Holz D. E., Linder E. V., 2005, ApJ, 631, 678
Hounsell R. et al., 2018, ApJ, 867, 23
Jeffrey N. et al., 2021, MNRAS, 505, 4626
Jönsson J. et al., 2010, MNRAS, 405, 535
Kainulainen K., Marra V., 2009, Phys. Rev. D, 80, 123020
Kainulainen K., Marra V., 2011a, Phys. Rev. D, 83, 023009
Kainulainen K., Marra V., 2011b, Phys. Rev. D, 84, 063004
Kaiser N., Peacock J. A., 2016, MNRAS, 455, 4518
Kessler R., Scolnic D., 2017, ApJ, 836, 56
Lemos P., Lee E., Efstathiou G., Gratton S., 2019, MNRAS, 483, 4803
Lemos P. et al., 2021, MNRAS, 505, 6179
Lemson G., Virgo Consortium T., 2006, preprint (astro-ph/0608019)
Macaulay E. et al., 2020, MNRAS, 4059, 4051
Mandelbaum R. et al., 2005, MNRAS, 361, 1287
Mandelbaum R., Seljak U., Cool R. J., Blanton M., Hirata C. M., Brinkmann J., 2006, MNRAS, 372, 758
Mandelbaum R., Seljak U., Hirata C. M., 2008, J. Cosmol. Astropart. Phys., 2008, 006 (M08)
Marra V., Quartin M., Amendola L., 2013, Phys. Rev. D, 88, 063004
Menard B., Scranton R., Fukugita M., Richards G., 2010, MNRAS, 1039, 1025
Ménard B., Kilbinger M., Scranton R., 2010, MNRAS, 406, 1815
Metcalf R. B., Silk J., 1999, ApJ, 519, 1
Muñoz-Cuartas J. C., Macciò A. V., Gottlöber S., Dutton A. A., 2011, MNRAS, 411, 584 (MC11)
Navarro J., Frenk C. S., White S. D. M., 1996, AJ, 462, 563
Nicolas N. et al., 2021, A&A, 649, A74
Oguri M. et al., 2018, PASJ, 70, S26
Phillips M. M., 1993, ApJ, 413, L105
Riess A. G. et al., 2007, ApJ, 659, 98
Riess A. G. et al., 2018, ApJ, 853, 126
Riess A. G., Casertano S., Yuan W., Bowers J. B., Macri L., Zinn J. C., Scolnic D., 2021, ApJ, 908, L6
Schneider P., 1985, A&A, 143, 413
Scolnic D. M. et al., 2018, ApJ, 859, 101
Seljak U., Holz D. E., 1999, A&A, 351, 10
Shah P., Lemos P., Lahav O., 2021, Astronomy and Astrophysics Reviews, 29, 9
Sheldon E. S. et al., 2004, AJ, 127, 2544
Smith M. et al., 2014, ApJ, 780, 1
Smith M. et al., 2020, AJ, 160, 267
Springel V. et al., 2005, Nature, 435, 629
Tallada P. et al., 2020, Astron. Comput., 32, 100391
Tripp R., Branch D., 1999, ApJ, 525, 209
Tröster T. et al., 2021, A&A, 649, A88
Van Uitert E., Hoekstra H., Velander M., Gilbank D. G., Gladders M. D., Yee H. K., 2011, A&A, 534, A14
Weinberg S., 1976, ApJ, 208, 1
Weingartner J., Draine B., 2001, ApJ, 548, 296
Wong K. C. et al., 2020, MNRAS, 498, 1440
Wright C. O., Brainerd T. G., 2000, ApJ, 534, 34
Zhan H., Tyson J., 2018, Rep. Prog. Phys., 81, 066901

APPENDIX A: SPECIFIC HALO PROFILES

In this appendix, we summarize analytical results for the lensing magnification by certain halo profiles.

A1 Singular isothermal sphere

The singular isothermal sphere (SIS) is derived from the assumption that dark matter haloes are thermalized with a homogeneous temperature. The density profile is

$$\rho_{\rm SIS}(r) = \frac{\sigma_v^2}{2\pi G r^2}, \tag{A1}$$

where $\sigma_{\rm v}$ is the isotropic velocity dispersion of dark matter. The mass inside r_{200} is $M_{200} = \frac{800\pi}{3}\rho_{\rm c} r_{200}^3$, and if this is assumed to be fully virialized, we can obtain the velocity dispersion as a function of M_{200} from the virial theorem as

$$\sigma_{\rm v}^6 = \frac{\pi}{6} 200 \rho_{\rm c} M_{200}^2 G^3. \tag{A2}$$

It is then straightforward to integrate $\rho_{\rm SIS}$ for the surface density, and we obtain convergence and shear as

$$\kappa_{\rm SIS} = \gamma_{\rm SIS} = \frac{G\sigma_{\rm v}^2}{2\Sigma_{\rm c}} \frac{1}{b} \tag{A3}$$

(see e.g. Bartelmann & Schneider 2001, equation 3.19). Hence, the magnification is

$$\mu = \frac{\theta}{\theta_{\rm E} - \theta}, \tag{A4}$$

where

$$\theta_{\rm E} = \frac{4\pi\sigma_v^2}{c^2} \frac{D_{\rm ds}}{D_{\rm s}} \tag{A5}$$

is the Einstein radius of the halo.

We see that at large radii, $\Delta\mu = \mathcal{O}(\theta^{-1})$ and so in the case of a uniform surface density of lensing galaxies with overlapping haloes, the total lensing amount does not converge as we extend our field radius. Nevertheless, we use the SIS profile as a useful control profile to compare with others that are better motivated.

A2 $\beta = 1$

A form of softened isothermal sphere, the convergence has a closed form expression for $\beta = 1$, which is

$$\kappa_{\beta=1} = \begin{cases} \frac{4\delta_{\rm c}\rho_{\rm c} r_{\rm s}}{\Sigma_{\rm c}\sqrt{(1-x^2)^2}} \operatorname{arctanh}\left(\sqrt{\frac{1-x}{1+x}}\right) & x < 1 \\ \frac{4\delta_{\rm c}\rho_{\rm c} r_{\rm s}}{\Sigma_{\rm c}\sqrt{(x^2-1)^2}} \arctan\left(\sqrt{\frac{x-1}{1+x}}\right) & x > 1, \end{cases} \tag{A6}$$

where $x = b/r_{\rm s}$ is the dimensionless impact parameter in units of the scale radius.

A3 NFW halo

Navarro et al. (1996) proposed an NFW profile to empirically fit their N-body simulations of collapsed dark matter haloes over a wide range of masses. The density profile is

$$\rho_{\rm NFW}(r) = \frac{\delta_{\rm c}\rho_{\rm c}}{\left(\frac{r}{r_{\rm s}}\right)\left(1+\frac{r}{r_{\rm s}}\right)^2} \,. \tag{A7}$$

The scale radius $r_{\rm s} = r_{200}/c$, where the concentration parameter c is thought to be weakly dependent on the halo mass, with smaller haloes being more concentrated (Navarro et al. 1996).

The profile is softer than the isothermal sphere at small radii, and turns over at $r_{\rm s}$ to r^{-3}. Although its total mass diverges logarithmically, we may equate $M_{200} = M(r_{200})$ and obtain

$$\delta_{\rm c} = \frac{200}{3}\frac{c^3}{\ln(1+c) - c/(1+c)} \,. \tag{A8}$$

Wright & Brainerd (2000) find that

$$\kappa_{\rm NFW} = \begin{cases} \frac{2r_{\rm s}\delta_{\rm c}\rho_{\rm c}}{\Sigma_{\rm c}(x^2-1)}\left\{1 - \frac{2}{\sqrt{1-x^2}}\operatorname{arctanh}\sqrt{\frac{1-x}{1+x}}\right\} & x < 1 \\ \frac{2r_{\rm s}\delta_{\rm c}\rho_{\rm c}}{3\Sigma_{\rm c}} & x = 1 \\ \frac{2r_{\rm s}\delta_{\rm c}\rho_{\rm c}}{\Sigma_{\rm c}(x^2-1)}\left\{1 - \frac{2}{\sqrt{x^2-1}}\arctan\sqrt{\frac{x-1}{x+1}}\right\} & x > 1. \end{cases} \tag{A9}$$

The shear is

$$\gamma_{\rm NFW} = \begin{cases} \frac{r_{\rm s}\delta_{\rm c}\rho_{\rm c}}{\Sigma_{\rm c}} g_<(x) & x < 1, \\ \frac{r_{\rm s}\delta_{\rm c}\rho_{\rm c}}{\Sigma_{\rm c}}\left[\frac{10}{3} + 4\ln\frac{1}{2}\right] & x = 1, \\ \frac{r_{\rm s}\delta_{\rm c}\rho_{\rm c}}{\Sigma_{\rm c}} g_>(x) & x > 1 \,, \end{cases} \tag{A10}$$

where

$$\begin{aligned} g_< &= \frac{8\operatorname{arctanh}\sqrt{(1-x)/(1+x)}}{x^2\sqrt{1-x^2}} + \frac{4}{x^2}\ln\frac{x}{2} \\ &\quad - \frac{2}{(x^2-1)} + \frac{4\operatorname{arctanh}\sqrt{(1-x)/(1+x)}}{(x^2-1)(1-x^2)^{1/2}}, \\ g_> &= \frac{8\arctan\sqrt{(x-1)/(1+x)}}{x^2\sqrt{x^2-1}} + \frac{4}{x^2}\ln\frac{x}{2} \\ &\quad - \frac{2}{(x^2-1)} + \frac{4\arctan\sqrt{(x-1)/(1+x)}}{(1-x^2)^{3/2}}. \end{aligned} \tag{A11}$$

A4 Hernquist profile

For the Hernquist profile ($\beta = 3$), the convergence is

$$\kappa_{\rm Hern} = \frac{\delta_{\rm c}\rho_{\rm c} r_{\rm s}}{\Sigma_{\rm c}(1-x^2)^2}\left(\left(2+x^2\right)S(x) - 3\right) \,, \tag{A12}$$

$$S(x) = \begin{cases} \frac{1}{1-x^2}\log\left(1+\sqrt{(1-x^2)/x}\right) & x < 1 \,, \\ \frac{1}{x^2-1}\arccos 1/x & x > 1 \,, \end{cases} \tag{A13}$$

as given by Hernquist (1990).

APPENDIX B: ANALYTIC DERIVATION OF $\sigma_{\rm LENS}$

Gravitational lensing is a two-body interaction. We may estimate the interaction rate per source as $\propto n_c V$, where n_c is the comoving number density and V is an applicable comoving volume. Therefore, we may expect $\sigma_{\rm lens} \propto V^{1/2}$ if n_c is approximately constant and galaxies are randomly distributed. The applicable volume should be related to the lensing efficiency squared (i.e. the 'cross-section' of the interaction) integrated over the distance to the source.

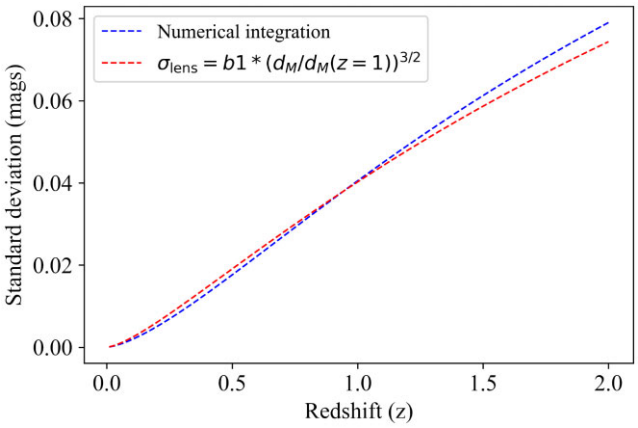

Figure B1. $\sigma_{\rm lens}$ computed by numerical integration with parameters $M_{200} = 10^{11}\,{\rm M}_\odot$, $c = 6$, $n_c = 2.5\ {\rm Mpc}^{-3}$, together with the approximate formula (B13) for $b_{\rm min} = r_{\rm sc}$.

A general formula for the variance of the lensing convergence due to haloes has been derived in Kainulainen & Marra (2009, 2011a), who used the same density model as we do. We summarize their derivation, and explicitly integrate it for the case of NFW haloes.

It is convenient for this calculation to split the convergence as

$$\kappa \equiv \kappa_H + \kappa_E \,, \tag{B1}$$

where

$$\kappa_E = -\int_0^{r_s} \frac{3\Omega_{M,0}}{2c^2} H_0^2 (1+z(r)) d_{\rm lens}(r) {\rm d}r \tag{B2}$$

is the 'empty beam' value corresponding to maximum demagnification, which is constant for a given source distance. $d_{\rm lens} \equiv \frac{r(r_s - r)}{r_s}$ is the lensing efficiency for a source at comoving distance r_s and a lens at r. The convergence due to matter haloes along a given LOS to a source may be written as the sum of contributions discretized over N_S bins in comoving distance $\{r_i\}$ and N_R bins in comoving impact parameter $\{b_m\}$:

$$\kappa_H = \sum_{i=1}^{N_S}\sum_{m=1}^{N_R} k_{im}\kappa_{1,im} \,. \tag{B3}$$

The k_{im} are random number counts of lensing haloes in the comoving volume defined by the interval $(r_i,\ r_i + \Delta r_i)$ and $(b_m,\ b_m + \Delta b_m)$ where the binning is arbitrary, but small enough such that the convergence $\kappa_{1,\,im}$ of single haloes can be taken to be a fixed value over the bin.

The k_{im} have Poisson statistics

$$P(k_{im}) \sim {\rm Poisson}(\Delta N_{im}) \tag{B4}$$

$$= \frac{(\Delta N_{im})^{k_{im}}}{k_{im}!}\exp -\Delta N_{im} \,, \tag{B5}$$

where the Poisson parameter is the expectation of the number of haloes in each bin

$$\Delta N_{im} = n_c(2\pi b_m \Delta b_m)\Delta r_i. \tag{B6}$$

Photon conservation is ensured by the requirement that the matter density of haloes averages to the homogeneous matter density $\Omega_{\rm m}$.

B1 $\sigma_{\rm lens}$ for a general halo profile

For simplicity here, we take all haloes that have the same mass and parameters – an extra bucketing scheme can be easily introduced to

generalize this if desired. We also assume that the comoving number density of haloes is constant with time, the matter distribution along LOSs to supernovae has the same distribution as randomly drawn LOSs, and the Poisson numbers k_{im} are uncorrelated.

The assumption of a randomly drawn and unbiased LOS, while consistent with the 'stochastic' treatments of Holz & Linder (2005), Jönsson et al. (2010), and Kainulainen & Marra (2009), is not trivial: SN Ia are not located randomly in empty space but instead in galaxies. To the extent that galaxies cluster (i.e. exhibit positive spatial correlation of their number density), SN Ia may be expected to lie preferentially in overdense regions, and the Poisson numbers k_{im} will indeed be correlated. Kainulainen & Marra (2011b) examined spatial correlations in this model by using the halo model, which splits the contribution into one-halo (peak) and two-halo (background) components, and found that the additional contribution to the variance due to the two-halo term was relatively small. However, taking into account mass variability and potential halo substructure, there formulae stated here should be seen as a *lower bound* for the true lensing dispersion.

Equation (B3) is the weighted sum of uncorrelated (but not identically distributed) Poisson random numbers k_{im}. We can therefore write

$$\mathrm{Var}(\kappa) = \sum_{im} \kappa_{1,im}^2(z_s)\Delta N_{im}, \tag{B7}$$

where we have used the properties of variance that $\mathrm{Var}(X_i + c) = \mathrm{Var}(X_i)$ for any random variable X_i and constant c, $\mathrm{Var}(a_i \sum X_i) = \sum a_i^2 \mathrm{Var}(X_i)$ for any uncorrelated random variables, and specifically for the Poisson distribution $\mathrm{Var}(k_{im}) = \Delta N_{im}$.

Converting the sum into an integral, we have (see also equation 70 of Kainulainen & Marra 2011a)

$$\sigma_{\rm lens}^2 = 2\pi n_c \left[\frac{3}{2}\Omega_{m,0}\frac{H_0^2}{c^2}\right]^2 \int_0^{r_s} \mathrm{d}r\, d_{\rm lens}^2(r, r_s)(1+z(r))^2 \int_{b_{\rm min}}^{b_{\rm max}} b\mathrm{d}b \left(\int_b^{b_{\rm max}} \frac{2x\mathrm{d}x}{\sqrt{x^2-b^2}}\frac{\rho(x,r)}{\bar{\rho}_m}\right)^2, \tag{B8}$$

where $b_{\rm min}$ and $b_{\rm max}$ are the arbitrary comoving cutoff radii imposed to regularize the integrals ($b_{\rm max}$ may be taken to be a truncation radius). The latter integral is the comoving halo surface density at impact parameter b normalized to units of the average matter density $\bar{\rho}_m$. We see that the volume element enters via the product $d_{\rm lens}^2 \mathrm{d}r$.

B2 $\sigma_{\rm lens}$ for the NFW halo profile

We use the formula for $\kappa_{\rm NFW}$ specified in Appendix A and define $f_c = 1/(\log(1+c) - c/(c+1))$. In the limit $x \gg 1$, we have

$$\kappa_{1,im} \simeq \frac{2GM_{200}f_c}{c^2} d_{\rm lens}(r_i, r_s)\frac{1}{b_m^2}, \tag{B9}$$

and in fact this will be an adequate proxy for our purposes. c in the denominator is the speed of light. The proportionality to $1/b^2$ is due to $\rho(r) \propto 1/r^3$ for the NFW halo at large r.

Substituting this into equation (B8)

$$\sigma_{\rm lens}^2 = A \times I, \tag{B10}$$

where the constant of proportionality

$$A = \left(\frac{2GM_{200}f_c}{c^2}\right)^2 2\pi n_c, \tag{B11}$$

and

$$I = \int_0^{r_s} \mathrm{d}r \int_{b_{\rm min}}^{b_{\rm max}} \mathrm{d}b \frac{r^2(r_s-r)^2}{r_s^2}\frac{1}{b^3}. \tag{B12}$$

All variables are expressed as comoving distances. With the final assumption that $b_{\rm max} \gg b_{\rm min}$ are fixed and not functions of r, we arrive at

$$\sigma_{\rm lens} \simeq \sqrt{\frac{A}{60}}\frac{r_s^{3/2}}{b_{\rm min}}. \tag{B13}$$

In fact, the integral without assuming the large x approximation can be done numerically, in which case we find $b_{\rm min} \simeq r_{\rm sc} = r_{200}/c$, as shown in Fig. B1.

The behaviour $\sigma_{\rm lens} \propto r^{3/2}$ is generic provided our assumptions hold, and we checked our formula matches that of a randomly generated galaxy catalogue. We have also checked the formula against $\sigma_{\rm lens}$ calculated from a galaxy catalogue generated from the Millennium Simulation by Henriques et al. (2012). There is a modest extra variance, increasing with distance, indicating the spatial correlation of galaxies. However, when centring the LOSs on random *galaxies*, we find that $\sigma_{\rm lens}$ is larger than our formula by ~ 50 per cent at $z = 1$.

It is this last point that has interesting implications for supernova cosmology: the Pantheon SN Ia may be special if they lie preferentially where the matter density and clustering are different than the background average.

This paper has been typeset from a TEX/LATEX file prepared by the author.